Master of Science Thesis

Development of novel anion exchange membranes for alkaline water electrolysis with employment of DC electric field

Jasna Đurović

Delft University of Technology

TU Delft

Delft University of Technology
Faculty of Applied Sciences

Development of novel anion exchange membranes for alkaline water electrolysis with employment of DC electric field

Instructor:	*Asst Prof* Hanieh Bazyar	**Student:**	Jasna Đurović
Teaching Assistant:	*Postdoc* Thanos Papageorgiou	**Student Number:**	5829984

Project Duration: September, 2023 - June, 2024

TU Delft

Preface

Over the past nine months, my MSc thesis project has been both challenging and exciting. This period has taught me about patience, determination, and the many difficulties present in a researcher's life.

Initially, I began working on a project focused on electrospinning in the P&E department (ME). However, due to unlucky lab events I eventually transitioned to a new topic, which is presented in this report, conducted in the TP department at the Faculty of Applied Sciences.

Despite the difficulties of changing my thesis project and the various obstacles we encountered, I thoroughly enjoyed my time in the lab. Those who knew me during this period were aware of the challenges I faced. However, the support and help of the people around me made it possible to overcome these stressful times. Without all of you, this would be impossible.

In that name I would like to thank everyone who has been part of this last phase of my academic studies.

First of all, I would like to thank Hanieh Bazyar for all the supervision I received during the thesis. Your kind guidance and feedback helped me immensely.
I would also like to express my big gratitude to my daily supervisor, Thanos Papageorgiou for all the help and guidance I received during the last 9 months. Thank you for answering all my questions, whether clever or not, anytime I needed.
I would also like to thank Prof. David Vermaas and Dr. Baris Kumru for being part of my committee and reading my report.
I want to express my gratitude to the technicians from the ASM department, Aleksandra Kondakova and Sietse Kuipers, for their infinite patience and assistance during my measurements over the past few months.

I would also like to thank the people from my research group, specially to my lab mate Kalai whose friendship and support made the lab work much easier and joyful.
I would like to thank to all of my friends, both from Delft and Serbia, for being there for me whenever I needed a call and a warm conversation. Your support meant a world to me.
Finally, I want to thank my parents and my brother for believing in me and helping me every stop along the way. This thesis I dedicate to you.

Jasna Đurović

Abstract

Nowadays, Hydrogen production is an important piece in energy transition system and holds a significant place in various industries. This gas is precursor for producing valuable compounds in the chemical industry and serves as a clean fuel, enabling efficient electricity generation when used with fuel cells. [1] However, majority of its production still relies on reforming and gasification of non-renewable sources. A sustainable pathway for Green Hydrogen production through water electrolysis already exists. However, scaling up and commercializing this technology represents challenge in meeting global demand, which was reported to be around 95 million tonnes in 2022. [2] Commercially available water electrolysis done in acidic environment is robust, however rather expensive. Anionic Exchange Membrane Water Electrolysis (AEMWE) is available alternative, but still not fully developed to be used on big industrial scales. AEMWE offers reduced cost as this technology does not require usage of expensive noble metal catalysts used in acidic electrolysis. Focus of the AEMWE research area is Anionic exchange membrane (AEM) as high values of conductivity of hydroxide ions could lead to fair technical competitiveness of alkaline and acidic electrolysis. [3] However, the majority of currently available AEMs lack the desirable properties, such as mechanical/alkaline stability as well as anionic conductivity.

One of the promising novel techniques for membrane fabrication consists of membrane casting with employing DC electric field, which enhances charged polymer channel orientation. [4] Reports have shown that polymer ion channels in random direction may cause slower migration and consequently lower values for conductivity. On the other hand, it has been proven that DC treated membranes can yield up to three times higher values for conductivity of OH^- ions. [5] Therefore, researching optimal DC values for casting significantly impacts electrochemical cell performance. [5]

This thesis report focuses on fabrication, characterisation and performance evaluation of the cast membranes with DC empolyment, prepared from cationic polymer kindly provided from industrial collaborator. Furthermore, an attempt will be made to assess competitiveness between produced and commercially available membranes. Finally, future suggestions for research directions and alternative membrane fabrication techniques will be provided, as these could offer valuable insights for further exploration in this field.

Contents

List of Figures

Nomenclature

Abbreviations

Abbreviation	Definition
AEM	Anionic Exchange Membrane
AWE	Anionic Water Electrolysis
AEMWE	Anionic Exchange Membrane Water Electrolysis
CP	Chronopotentiometry
CV	Chrono Voltammetry
DSC	Differential scanning calorimetry
FTIR	Fourier-transform infrared spectroscopy
GPC	Gel Permeation Chromatography
GHG	Greenhouse gasses
HER	Hydrogen Evolution Reaction
IEM	International Energy Agency
IEC	Ionic Exchange Capacity
LSV	Linear Sweep Voltammetry
LGS	Linear Galvanodynamic Sweep
MW	Molecular Weight
MEA	Membrane Electrode Assembly
NMR	Nuclear Magnetic Resonance
OER	Oxygen Evolution Reaction
PEM	Proton Exchange Membrane
PEMWE	Proton Echange Membrane Water Electrolysis
TGA	Thermogravimetric Analysis
WUR	Watet Uptake Ratio
XPS	X-ray photoelectron spectroscopy

1 Introduction

Over the past few decades, producing hydrogen in a cost-effective, resilient, and sustainable manner has been a challenge for an energy transition and the global goal of zero greenhouse gas emissions (GHG). [6] Estimation was that in 2021, commercial production of hydrogen almost completely relied on non-renewable sources of energy such as natural gas, coal and oil with almost 96% share in the total hydrogen production. [2] The other 4% coming from electrolysis showed considerable efforts of the scientific community to optimize, improve and make electrolysis effective and cost competitive comparing to other mature and well-known technologies.

Current research revolving water electrolysis has centered on proton exchange membrane (PEMWE). This technology has proven to achieve high current and power densities. [6] However, PEMWE requires presence of noble catalysts such as Pt or Ir/Ru oxide. This makes PEMWE rather expensive and alternatives are required. [3]

Anionic exchange membrane water electrolysis (AEMWE) offers great advantage of using low cost transition metal catalysts, such as Nickel, with presence of anionic exchange membrane (AEM). AEMs are made from suitable functionalized ionic polymers which enable conducting hydroxide ions. In comparison with the traditional alkaline electrolyzers, in which concentrated KOH solutions are needed, AEMWE can operate with low concentration of alkali or even distilled water. [3] Hydroxide ions produced on the cathode are available for the ionic transfer through the membrane and consequently, chemical transformation to oxygen can occur on the anodic side. However, most of the research regarding AEMWE has been done in presence of 1M KOH, as supporting OH^- ion enable lower overpotentials and higher efficiencies of the electrolysis systems. [3] These features attract a lot of attention to the technology itself, but knowledge about appropriate materials used for membrane manufacturing is still very limited and represents a big challenge for commercialization. [3]

Most AEMWEs have poor current densities, below 1 A/cm^2 at 2 V, and low cell durability with less than 100 h. Membrane polymer selection is a crucial part of AEMWE system, which can potentially address the above-mentioned shortcomings. [7] Anionic Membranes for AEMWE need to be able to (1) conduct hydroxide ions, (2) prevent electrons from passing through the internal circuit, and (3) inhibit gaseous products migration between the two compartments of the electrochemical cell. [8] Therefore, great efforts have been made towards manufacturing membranes with high OH^- conductivity, durability, ion exchange capacity, chemical stability, and good mechanical and thermal properties. [9]

Most of the AEMs today are fabricated with solution casting due to relative simplicity of the manufacturing process.[10] This method enables making amorphous structured membranes with appropriate thicknesses of around 30 –100 µm for water electrolysis. [11] AEMs ideally need high ionic conductivity and low resistances to yield the highest efficiencies of alkaline water electrolysis. Commercial AEMs, such as Sustainion® have shown values of conductivity of up to 80 mS/cm at room temperatures between 20-30 °C. However, as previously mentioned, these membranes do not yield satisfactory current densities in AEMWE systems. [12] Therefore, immense effort has been directed towards synthesis of novel anionic conductive polymers and new ways of membrane fabrication, which would enhance mentioned properties. In previous research, it has been shown that manipulation of polymer morphology

can be achieved with applying DC electric field while casting. [4]. Not only does this method improves the conductivity of membrane, but also enhances the alkaline stability. [4] This is mainly due to orientation of ionic channels which effectively accelerates the ion migration, increasing the conductivity. [5] Some studies have reported that conductivities of pristine and electrically treated membranes can differ up to three times, in favor of the latter ones. [5] Tailoring the anisotropic properties of the polymer structure is therefore beneficial, and will be of the interest in this thesis research.

As state-of-the-art literature suggests, anion exchange membranes have been mostly manufactured from polymers with poly-sulfone, polystyrene, poly(phenyl ether) or polyphenylene backbones, and ammonium, imidazolium, phosphonium or sulfonium ion exchange groups. [3, 13, 14] It is believed that ammonium cationic group has been the most studied and all that due to durability and high conductivity. [13]

In this work, polymer with ammonium cationic exchange groups, synthesized by the industrial collaborator of this project, will be used to fabricate electro-cast membranes. Voltage range applied will be between 0-3 V DC. Following this, membranes will be characterized and their performance will be evaluated in an electrochemical cell. The goal is to report the optimal fabrication parameters and roughly assess their comparability with commercially available products.

Hopefully, this thesis work will provide insights into the effects of a DC electric field on membrane morphology and macroscopic properties including ion conductivity, ion exchange capacity, thermal properties, as well as water uptake ratio.

2

Theoretical background

2.1. Importance of Hydrogen in energy transition

Hydrogen, a simple diatomic molecule gas represents a valuable compound not only in chemical industry but also other parts of the world's economy. In the recent years, research community's aspiration to increase hydrogen use for power and electricity production has been quite strong with the aim to contribute to the energy transition and global decarbonisation. Data given by International Energy Agency (IEM) for Global Hydrogen use **today** and estimated Global Hydrogen use by **end of 2030** (see Figure 2.2) shows that hydrogen is still insignificantly used as an energy source. The high cost of hydrogen and its production compared to non-renewable fuels are the primary obstacles disabling its further implementation in the energy sector. [6]

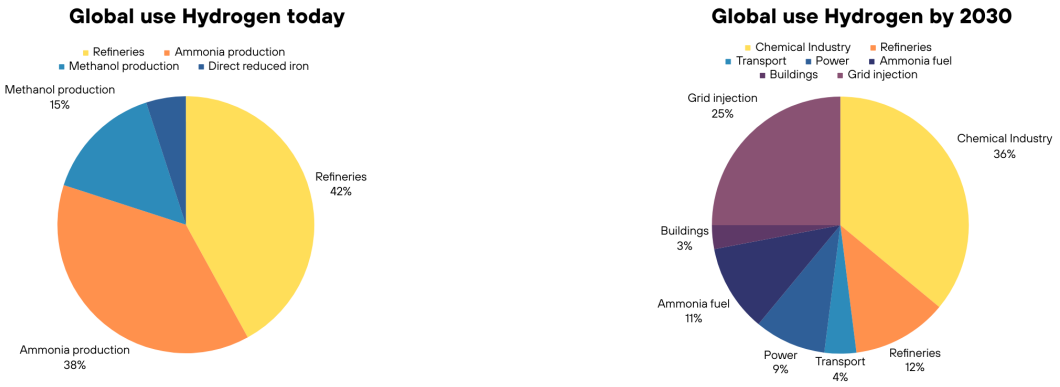

Figure 2.1: IEM adopted data for Global Hydrogen use today and by 2030; data adopted [15]

To understand how hydrogen participates in the energy and chemical cycles of the global economy, it is crucial to understand its life cycle through its production, storage and use.

Hydrogen can be produced from natural gas, through reforming, gasification of coal, or from renewable sources (solar and wind energy). Estimations for hydrogen production today claim that almost 96% comes from non-renewable sources, while the rest is produced with electrolysis, as shown in Fig.2.2. Predictions are that by 2050 hydrogen production through electrolysis will rise significantly to 22%, whereas new ways of producing, such as biomass hydrogen production will share almost a tenth of total H_2 production.

Considering intermittent fluctuating production peaks of electricity obtained from wind and solar energy, it is required to seek for long-term storage solutions. Hydrogen is shown as an excellent candidate, as its subsequent application for electricity production is closing the circle of sustainable power production. [16] However, both physical and material-based ways of storing hydrogen are quite complex considering low volumetric density and small molecular mass, enabling hydrogen to escape from storage systems in the atmosphere. [17] Hydrogen offers mobility in a sense of facilitated energy trans-

port, which is shown to be crucial for remote places on the earth which are away from standard systems of electrical grids [1].

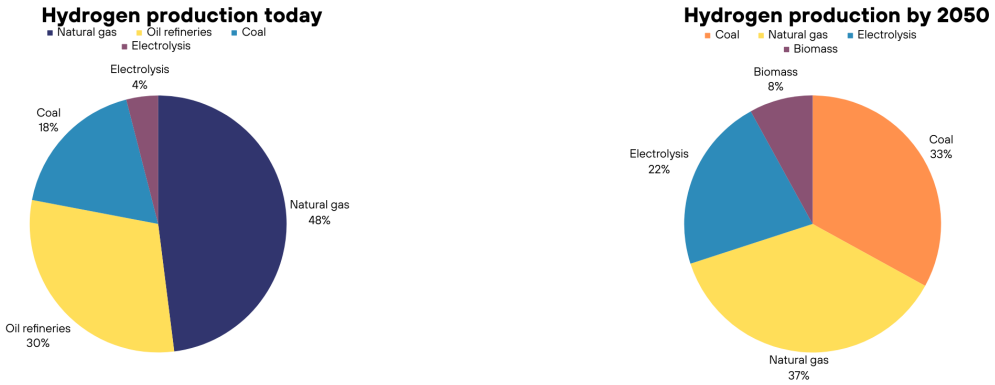

Figure 2.2: Hydrogen production technologies today and by 2050; data adopted [18]

Energy and hydrogen losses during life cycle described above are still considerable. If green hydrogen is produced through electrolysis with renewable energy, expected energy efficiency is around 70 %. During storage, loss of hydrogen is inevitable and differs depending on the type of the storage. Fuel cells achieve hydrogen conversion efficiencies ranging between 50% and 60%. Therefore, hydrogen from production, storage to utilization accounts for 65% energy loss. The necessity for hydrogen technology development is obvious. In spite of time-consuming and expensive future developments, this gas is deemed as a worth risk-taking choice [6].
To support the increasing demand for hydrogen production, academia's aim has been focused on examining efficient ways of producing it. Electrolysis stands out as a unique and reliable process that, with improved efficiencies, has the potential to significantly contribute to the world's energy infrastructure in the future. [17] Electrolysis driven by renewable energy with the simultaneous use of renewable input sources such as water, with no carbon dioxide/ GHG emissions stands out as one of the most promising technologies of the modern age. [1]

2.2. Water Electrolysis

Water electrolysis is the electrochemical process of decomposing water, utilizing electricity to produce hydrogen and oxygen as its primary products. Water splitting reaction takes place in electrolysis cell – electrolyzer, where redox half reactions of hydrogen and oxygen evolution happen on the cathode and anode, respectively. Water dissociates to H^+ and OH^- ions providing reactants for Hydrogen evolution reaction (HER) and Oxygen evolution reaction (OER), as shown in the equation 2.1.

$$H_2O \rightleftharpoons H^+ + OH^- \tag{2.1}$$

The half reactions occurring at each electrode are given below:

$$Cathode : 2H^+ + 2e^- \rightarrow H_2 \tag{2.2}$$

$$Anode : 2OH^- \rightarrow H_2O + \frac{1}{2}O_2 + 2e^- \tag{2.3}$$

Overall water splitting reaction is given in 2.4 .

$$H_2O + Electricity(237.2kJ/mol) + Heat(48.6kJ/mol) \rightarrow H_2 + 0.5O_2 \tag{2.4}$$

The reaction given happens at room temperature at minimum theoretical cell voltage of $1.23V$. However, experiments have shown that minimal cell voltage required is $1.48V$, where additional cell voltage is necessary to overcome kinetics and ohmic resistance of the electrolyte and components of electrolytic cell. [16]
The concept of electrolysis dates from late 18*th* century, when hydrogen was firstly produced with the use of electrostatic generator as the direct electricity source. [16] Since then, technology of electrolysis

has developed significantly, currently yielding production capacity of almost 11 GW in 2022. [19] Some estimations predict that by 2030, the capacity of green hydrogen production through electrolysis from renewable sources could increase up to 170-365 GW. Simultaneously, prediction is that by 2030, the price of green H_2 could potentially become equivalent to grey H_2 produced from natural gas. Technological advancements and the scaling up of production are expected to play key roles in achieving this cost reduction.[19]

One of the main approaches in increasing efficiency relies on minimising the various resistances of the electrolysis system. Apart from external electrical circuit resistances and electrochemical reaction resistances which imply overcoming overpotentials for electrochemical reaction activation, major bottleneck for electrolysis improvement lies in reducing transport related losses (ohmic losses). Transport resistances represent physical resistances in the electrochemical cell, such as gas bubbles formation on electrodes, resistances due to ionic transfer in electrolyte and membrane resistances. [1]

2.2.1. Types of water electrolysis systems

So far, three main types of water electrolysis have stood up as possible options for industrially viable hydrogen production; proton exchange membrane water electrolysis (PEMWE), alkaline water electrolysis (AWE) and anionic exchange water electrolysis (AEMWE). Operating principles are same for all three, however the main differences are based on the type of electrolyte, operating conditions and the ionic agents (OH^- and H^+). [16] For clearer overview and comparison of different water electrolysis systems please refer to Table 2.1.

	Alkaline water electrolysis (AWE)	Proton exchange membrane water electrolysis (PEMWE)	Anion exchange water electrolysis (AEMWE)
Anodic reaction	$2OH^- \rightarrow H_2O + 0.5O_2 + 2e^-$	$H_2O \rightarrow 2H^+ + 0.5O_2 + 2e^-$	$2OH^- \rightarrow H_2O + 0.5O_2 + 2e^-$
Cathodic reaction	$2H_2O + 2e^- \rightarrow H_2 + 2OH^-$	$2H^+ + 2e^- \rightarrow H_2$	$2H_2O + 2e^- \rightarrow H_2 + 2OH^-$
Electrolyte	KOH/NaOH (5M)	Solid polymer electrolyte	KOH/NaOH (1M)
Separator	Porous inorganic diaphragms	Polymer membrane	Polymer membrane
Charge carrier	OH^-	H^+	OH^-
Temperature range	70-90 $°C$	50-80 $°C$	40-60 $°C$
Type of catalysts	Ni coated perforated stainless steel	Pt/Ir based	Ni/Co/Fe based
Nominal current density [$mA/cm2$]	200-800	800-2500	200-2000
Efficiency [%]	50-78	50-83	57-59
Technology status	Mature	Commercialized	R & D

Table 2.1: Different types of water electrolysis; comparison [3, 16]

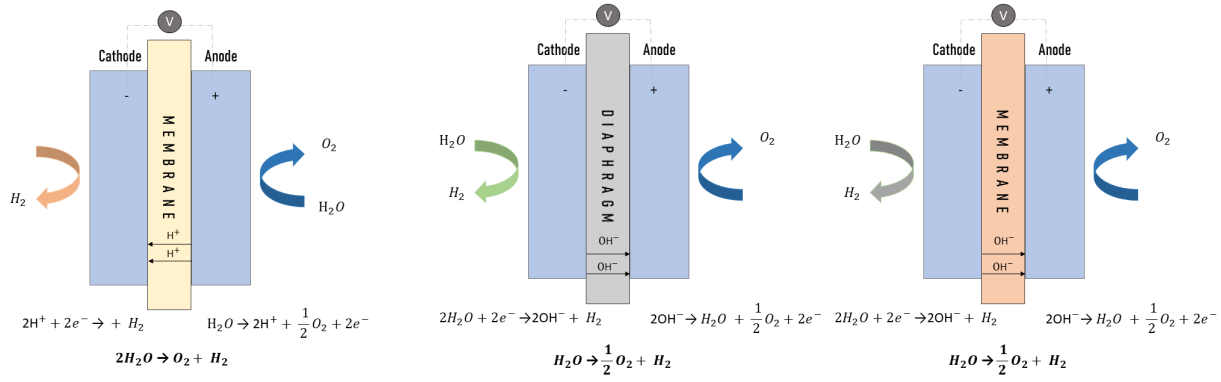

(a) PEMWE schematic **(b)** AWE schematic **(c)** AEMWE schematic

Figure 2.3: Schematics of different water electrolysis systems

PEMWE

PEMWE (see Figure 2.3a) is commercial type of electrolysis and performs well in acidic conditions with high efficiencies up to 80% with high nominal current densities, see table 2.1. However, PEMWE

requires expensive noble metal electrocatalysts ($IrO2$ and Pt), as well as perfluorinated membranes (Nafion), and therefore impose a big cost compared to other water splitting technologies. [20]

AWE
On the other hand, Alkaline water electrolysis (see Figure 2.3b) has potential for large-scale applications. However, due to existence of porous ceramic oxide diaphragms and low OH^- mobility compared to H^+, AWE achieves low current densities, up to 0.8 A/cm^2. [16] Presence of high concentration alkali (5M KOH/NaOH) implies sensitivity towards ambient CO_2, where formation of carbonate salts enhances clogging of diaphragm, and consequently reduces hydrogen production efficiency of AWE. [6, 16] A limitation of AWE systems is the generation of hydrogen with relatively low purity (around 99.9%) compared to alternative electrolysis technologies. This problem happens due to the permeation of hydrogen and oxygen across the solid diaphragm, leading to crossover between different sections of the cell. [16]

AEMWE
Compared to AWE, AEMWE (see Figure 2.3c) operates in presence of low concentration alkali (1M KOH) and uses anionic exchange membrane (AEM) as separator for OH^- conduction from cathode to anode. AEMWE is still in research phase, but possesses great potential due to low cost and high performance in terms of achieving higher current densities. [3] Although AEMWE electrodes can be made from inexpensive materials such as Ni and Co, the relatively slow kinetics of four-electron Oxygen evolution reaction and low stability of the anode materials challenges the development of this technology to its full potential. [21] Apart from electrode materials, improving anionic exchange membrane (AEM) remains a challenge due to its reduced mechanical stability at operational temperatures and lower ionic conductivity compared to PEM. [22] This last phenomenon is mainly attributed to the reduced mobility of OH^- compared to protons. [20]

Generally, electrolyzers can be subdivided into 2 groups; finite-gap and zero-gap. Finite-gap systems use porous separators (AWE, see Table 2.1) which require big thicknesses (>2mm) between cathode and anode to reduce crossover of produced gases, however at a cost of increased Ohmic losses. Zero-gap systems (PEMWE and AEMWE) offer reduced internal resistances as they employ thin polymeric membranes with low gas permeation, and will be out of interest in this research. [22]

2.3. Anionic Exchange Membranes

Currently available AEMs have shown relatively low ionic conductivity and low durability, consequently imposing major obstacles for development of AEMWE systems.[23] Polymer chemistry for developing novel anionic membranes is very important in overcoming existing problems and enhancing other critical parameters of AEMs such as ion-exchange capacity, mechanical stability, water uptake and swelling ratio.

AEMs are fabricated using polymers that possess cationic centers, bounded to the polymer backbones, which are capable of conducting hydroxide ions. State-of-the art suggests that quaternary ammonium cationic group has been researched the most in combination with poly(sulfone) and poly(styrene) backbones. [24] It has been shown that N-cyclic quaternary ammonium group shows much better alkaline stability than aliphatic quaternary ammonium salts. [20] Generally, hydrocarbon AEM polymers disable Hydrogen solubility and diffusion, and therefore allow utilization of thinner membranes (up to 100 μm). This is not the case in PEMWE, as PEM polymers allow gas diffusion and thinner membranes can impose safety issues in electrochemical cell. [25]

In alkaline environment, durability of quaternary amines in AEMs is endangered due to reactions of Hoffmann elimination, while piperidinium groups can participate in nucleophilic substitution and ring opening reactions. [26] Novel polymers with additional electronic protection and steric shielding of cationic centers can contribute to better AEM durability. [23]

Literature suggests that there is a big trade off between conductivity and dimensional stability of AEMs. To achieve high conductivity, AEM should have sufficiently high number of charged sites, which is reflected through ion exchange capacity (IEC, [mmol/g]). [20] However, membranes with high IECs show higher water uptake (WU) and water uptake ratio (WUR) due to increased polymer chain repulsion within the membrane body. Higher WU and WUR affect mechanical and dimensional stability negatively.

[14] Additionally, higher WU/WUR can reduce ion selectivity and increase ion crossover which is highly undesirable in operational electrochemical cell.

Hence, achieving optimal performance of AEMs requires selecting a polymer with mechanically robust backbone and carefully balanced type, quantity, and placement of charged centers within the polymer structure.

Up to this date, synthesised anionic exchange polymers failed in delivering conductivities above 100 mS/cm, and satisfactory mechanical stabilities above 60 $^\circ$ C. [23] To further enhance properties of AEMs, literature suggested possible ways of manipulating polymer morphology [4];

- Cross-linking of polymer
- Composite membranes
- Electrostatic alignment of polymer chains

Cross-linking creates chemical bonds between polymer chains, helps with reducing WU/WUR and ideally maintains high conductivity. Cross-linking can be physical (ion-ion interaction, Van der Waals interactions) or chemical (covalent bonding). If cross-linking is prominent, ionic channels for ion transfer can become blocked which decreases conductivity. Overall, cross-linking positively affects mechanical stability of AEMs, which is especially important for thin (less than 50 μm) membranes which operate in presence of high differential pressures in AEMWE. [23]

There are different ways of making organic/inorganic composite AEMs; often mentioned are mixed matrix membranes with embedded inorganic nano-particles (metal ions, metal oxides, fictionalized nano-particles, graphen oxide, etc.) into anionic exchange polymer. Other option is making membranes with inert porous base filled with anionic exchange polymer. Composite membranes promise increased tensile strength and better alkaline stability. [23]

Apart from these, one relatively novel approach is enhancement of the ionic channel orientation by employing DC (direct current) electric field while casting. In presence of electric field, functional cationic groups form ion channels which lower the transport resistance of AEM and facilitate hydroxide conductivity. [5]

2.4. Membrane Fabrication Methods

2.4.1. (Electro-)Casting method

Casting method is vastly used for manufacturing commercial membranes from viscous liquid polymer solutions. Casting allows preparation of compact membranes with different shapes, sizes and textures on moving or stationary surfaces. [27] A casting solution consists of a polymer and solvent, but various additives and co-solvents can be included to modify properties and influence phase separation within the membrane. Concentration of the polymer solution is a critical parameter which determines the membrane properties; low concentrations lead to thin and porous membranes, while high concentration of polymer produce membranes with dense structure, typically used for reverse osmosis, gas separation etc.[10] Usual polymer concentration in the casting solution is 15-20 %.

For AEMs, casting solution consists of positively charged polymer and suitable solvent. Regular casting yields dense AEMs with randomly entangled polymer chains, see Figure 2.4 (a). However, as reported, electric field-assisted casting helps with aligning anisotropic properties of polymer chains within the membrane, see Figure 2.4 (b). [28] Under electric field, polymer chains aggregate and from linear channels which facilitate ion conductivity. [29] Casting with employment of DC electric field requires a choice of dielectric solvent in order to enable conformational movement of polymer chains. [30] AEM polymer chains carry positive charges and are paired with counterions in the system. As a result, these positive and negative groups form dipoles that move when an electric field is applied. The movement of these dipoles at a specific angle within the electric field generates a current, which can be monitored over time to identify different phases in the alignment of the polymer chains. Initially, the charged chains respond quickly to the presence of the field, resulting in a high current. After certain amount of time, the current gradually decreases as the number of dipoles available for movement is reduced, eventually obtaining stable value. [31]

The application of an electric field during casting induces the formation of crystalline structures, resulting in a decrease in free volume within the material. This tighter microstructure disables the diffu-

sion of hydrogen and oxygen which is crucial for AEM applications. [30] Block copolymers containing charged hydrophilic sites attached to a hydrophobic backbone have shown a tendency for assembly in the casting solution and the formation of ionic channels. [30, 32]

Different voltages yield different degrees of crystallinity. However, extremely high potentials can affect polymer solution viscosity due to electroviscocus effect with simultaneous solvent electrolysis between casting blades. Depending on how positive and negative potentials are placed during membrane

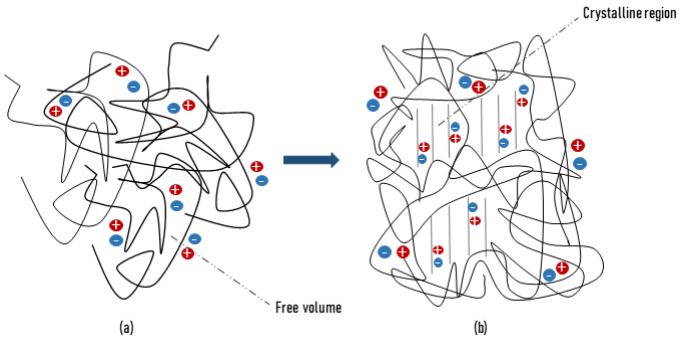

Figure 2.4: Formation of crystalline phases upon application of electric field during casting

casting, alignment of polymer chains can be in-plane or through-plane. However, many applications including water electrolysis, require through-plane alignment for increased conductivity. [32] Hence, this type of morphology will be out of interest in this study. Electro-casting method promises up to 3 times higher values for conductivity compared to untreated methods. [5] Due to simplicity of the preparation method and high potential for enhancing membrane properties, electro-casting with employment of DC electric field will be further researched.

2.4.2. Membrane Electrospinning

One of the novel techniques for membrane fabrication is electrospinning. This technique allows for the production of nanofibers, which could potentially achieve conductivity up to ten times higher than that of typically produced cast membranes, due to the increased surface area. [33]

Electrospinnig is a voltage-driven process which yields polymer nanofibers. This occurs when electrostatic forces at the top of the needle overcome surface tension of the solution. At this point Taylor cone is transforming into stable jet which is then collected on the grounded metal plate/drum. Electrospinning provides dense macroscopic scale and loose microscopic scales and therefore shows great potential for the future membrane fabrication. [34] Electrospinning as a production technique largely depends on choice of the operating parameters such as applied electric field, distance between the needle and the collector, flow rate of the solution, needle diameter, solution concentration, relative humidity and temperature. [35] Co-electrospinning from solution with multiple polymers can be achieved with the aim of improving membrane properties, however ratio of the polymers then becomes one of the observed parameters. Optimizing and tuning all of these parameters is one of the most important tasks in order to produce uniform fibers, which will later influence membrane properties.

As electrospun membrane mats are often porous and not compact it is important to design dense membrane which will not allow permeation of gases like O_2 and H_2. There are multiple ways to achieve this, one of which is hot pressing multiple membrane mats. [11] Other way is making an electrospun mat of nanofibers of an ionic conducting polymer embedded in an inert polymer, where the inert polymer acts as mechanical support and positively affects swelling properties. [36] It has also been reported that co-electrospinning and crosslinking can positively affect mechanical stability of the polymers in nanofibers, however only when choosing the right ratio of polymers in the injecting solution or when choosing the right crosslinking agents. [11] [36]

Most of the AEMs today are fabricated with solution casting due to simplicity of the manufacturing process. However, this method without additional application of electric field does not allow control of the membrane morphology. [11] Therefore, electrospinning is researched as a possible way of anionic exchange membrane manufacturing. Sophisticated technology such as electrospinning allows

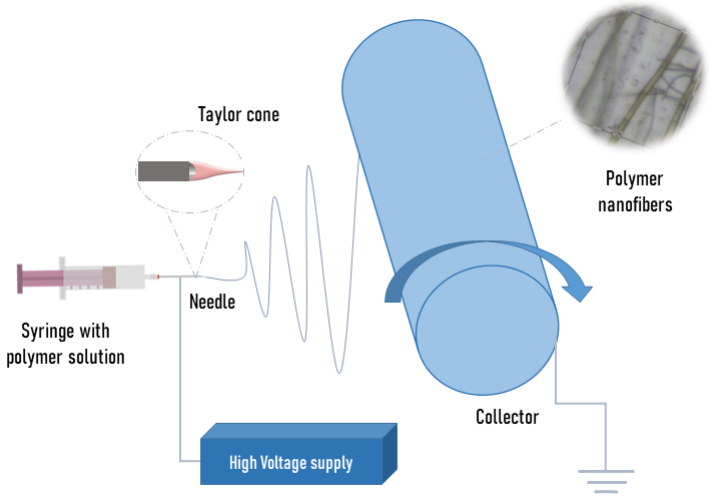

Figure 2.5: Electrospinning; schematic

uni-axial directed nanofibers production with fiber diameters in a range from 100-700 nm. Membrane mats produced this way exhibit higher conductivities due to large-sized ionic conduction channels and better mechanical properties due to existence of oriented fibers. [9]

2.5. Objectives of the Study and Research Question

Above mentioned theoretical introduction leads to the following problem definition:

"Present configurations of anionic exchange membrane electrolysis do not yield hydrogen production efficiencies comparable to PEMWE. However, the introduction of a novel polymer for membrane fabrication, coupled with the use of electrical field in casting, is expected to overcome the limitations of earlier materials in such way that these new membranes can outcompete commercially available products."

The goal of the thesis is to examine how different DC voltages applied during casting affect macroscopic properties of the membranes such as conductivity and ion exchange capacity. An attempt will be made to screen changes in membrane morphology and polymer chain alignment, as well as to link this phenomena with changes in membranes' performance. The results obtained from these experiments will hopefully answer the research question:

> What are the optimal DC electric voltage values used during electro-casting to achieve the most promising membrane properties for the polymer employed in this research?

Hopefully, this report will provide systematic overview of current state-of-the-art and prospects for future research in the area of electro-casting of anionic exchange membranes.

At the beginning of this Master Thesis project, we focused on electrospinning as a promising and innovative way for producing anionic exchange membranes. During the initial phase, considerable progress was made in electrospinning of the polymer used in this research (schematic of the equipment given in the Figure 2.5). However, due to technical issues, this part of the project had to be discontinued. Nevertheless, in the Section 6.0.3 we will show insights gained, highlighting electrospinning as a highly viable alternative for AEM production.

3

Experimental Methodology

3.1. Polymer characterization

The polymer used in this research was synthesized in-house by the project's industrial collaborator. It is a block co-polymer which possesses *quaternary ammonium cationic groups implemented in piperidinium structure, attached to aromatic backbone*, as shown in Figure 3.1.

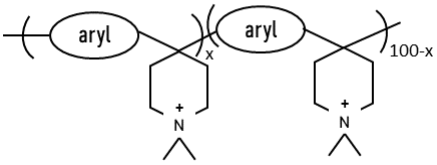

Figure 3.1: Functional groups of polymer assessed in this research

Due to confidentiality reasons, the exact structure of the polymer used will not be shown. However, the initial phase of this work will focus on characterization of the diblock copolymer through its molecular weight and glass transition temperature.

3.1.1. Molecular weight

The molecular weight of block-copolymers is usually determined through analysis of NMR spectra. However, due to lack of unique end-groups in the polymer structure, NMR was not sufficient and alternative had to be considered. [37]

Gel permeation chromatography (GPC)

GPC was performed with 2 mg/ml polymer solution in DMF (60 μl) on a *Prominence LC-20A* GPC equipped with *Agilent Technologies PLgel 5um MIXED* column (300 x 7.5mm). Molecular weight distributions were calculated relative to poly(ethylene-oxide) (PEO) calibration curve.

Rheology

Molecular weight of the polymer can be determined through measuring of intrinsic viscosity. While this method does not directly measure the weight of the polymer, it provides valuable insight into the size of the coil formed by the polymeric chain within the solution. Intrinsic viscosity refers to the theoretical viscosity of a polymer solution that is infinitely diluted. [38] It can be determined by extrapolating the graph of reduced viscosity versus concentration (C) for highly diluted solutions, as shown in the equation 3.1.

$$\eta_{intrinsic} = \lim_{C \to 0} \eta_{reduced}(C) \tag{3.1}$$

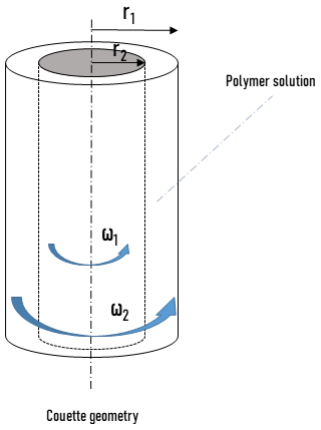

Figure 3.2: Couette geometry used for rheology measurements

Reduced viscosity is given by equation 3.2. Here, specific viscosity represents relative change of the polymer solution viscosity compared to the viscosity of the pure solvent, see equation 3.3. [39]

$$\eta_{reduced} = \frac{\eta_{specific}}{C} \tag{3.2}$$

$$\eta_{specific} = \frac{\eta - \eta_0}{\eta_0} \tag{3.3}$$

Here, η_0 is the viscosity of the pure solvent, and η is the viscosity of the polymer solution.

Diluted solutions of polymer in DMSO were prepared in following concentrations; 0.25 wt%, 0.5 wt%, 1 wt%, 1.5 wt%, 2 wt%, 2.5 wt%. The volume needed for the experimental part was high, around 30 ml, due to the utilization of Couette geometry, as shown in Figure 3.2.The viscosity was then determined with a *HR10 Hybrid Rheometer by TA instruments.*. A shear stress of 0.01 Pa was applied for a duration of 180 seconds using the aforementioned rheometer geometry. The values of absolute viscosity were then used to calculate the reduced viscosity and, finally, the values of intrinsic viscosity $[dL/g]$ were calculated via extrapolation.

3.2. Membrane fabrication

All membranes produced in this research were cast from 22wt% polymer solutions in DMSO (*Sigma-Aldrich*, ≥99.9%). The solutions were stirred for 3-4 hours at 40 °C and subsequently left overnight to settle in order to avoid the presence of bubbles during casting. The membranes were cast with an automatic *TQC Sheen* Dr Blade calibrated at a constant height of 35 μm. Smooth-surfaced stainless steel plates were employed as a casting surface, since previous trials showed that slight roughness of the plate can disable membrane pealing. Dr Blade was programmed to cast 170 mm length with casting rate of 0.1 mm/s. Temperature, pressure and relative humidity of the casting chamber were kept environmental. Average volume of the casting solution was around 3 ml, making a membrane sheet which could yield two to three membrane discs with 5 cm diameter. After casting, the polymer sheet on the stainless steel plate was dried in the oven at 80 °C overnight to remove the solvent. Following this, the plate was soaked in MiliQ water for 30 min to facilitate the peeling of the membrane off the plate . Soaked membrane was then placed in between polymethyl methacrylate (PMMA) plates and dried overnight in the vacuum oven at 40 °C. Finally, membranes with dry thicknesses of 30 $\pm$ 5 µm were ready for use.

A schematic of the (electro-) casting equipment is shown in Figure 3.3.

Same procedure described was followed when membranes were cast with/without employment of DC electric field. When electro-casting, input cables that provide potential (see (a) in Figure 3.3) had to be connected to the set-up. The casting blade was consistently set at a positive potential, whereas the stainless steel plate at a negative. Oscillometer and multimeter (see (b) and (c) in Figure 3.3) provided

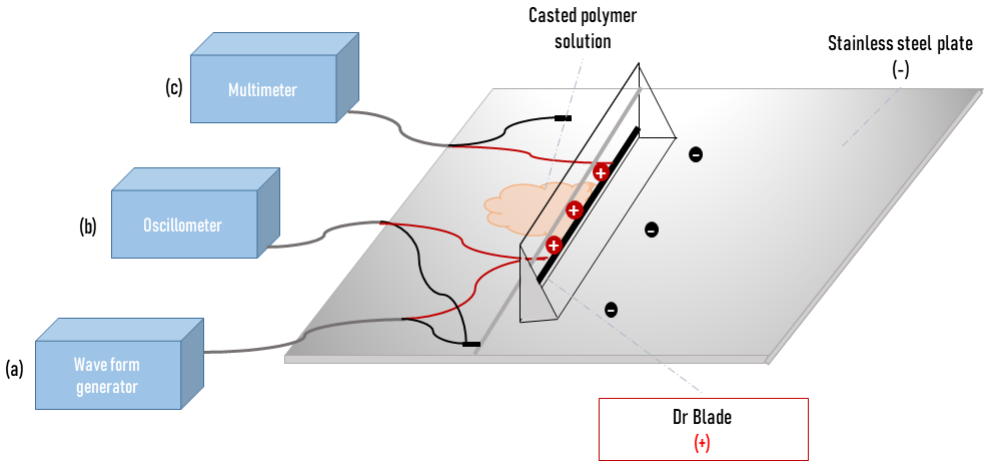

Figure 3.3: (Electro-)Casting; schematic

output information about current and potential waveforms in between plate and blade.

This research focused on electro-casting of membranes with offset voltages in range between 1-3V with 0.2V step. However, results and discussion section will also include results from membranes cast with 0-1V with 0.2V step prepared by my daily supervisor, Thanos Papageorgiou. This was decided, as complete understanding of membranes' behaviour can be better reviewed with an insight in wider range of applied DC voltages.

Finally, literature suggests that voltage applied across the height between blade and plate should be expressed in units of V/cm. However, since the casting height remained the same during the experiments, the membranes will stay labeled with their actual voltage values due to easier differentiation. [5]

3.3. Membrane characterization

3.3.1. Physical properties

Water Uptake ratio (WUR)

Water Uptake ratio (WUR) was measured by placing 1 cm diameter pieces of membranes in a vacuum oven at 40 °C for 2-3 hours. Thicknesses (L_{dry}) of dry membranes were measured with micrometer caliber before soaking in DI water. Membranes were soaked for 72 hr individually on the room temperature. After soaking, pieces of membranes were dried carefully with lint-free lab tissues, until excess water was removed. Again,thickness of wet membranes was measured L_{wet}. These recorded values were substituted in equation given below to obtain values for water swelling ratio (WUR).

$$WUR[\%] = \frac{L_{wet} - L_{dry}}{L_{dry}} * 100\% \tag{3.4}$$

Thermal properties

The thermal decomposition behavior of different membranes was determined through the **thermogravimetric analysis** (TGA) using *PerkinElmer Thermogravimetric Analayser 8000*. Before analysis, small pieces of membranes (few mg) were dried in the vacuum oven for 1 hour to remove excess of water and solvent. All measurements were performed from 30 to 800 °C with applied heating rate of 10 °C / min.

Thermal transitions in polymer materials provide valuable information about the polymeric material and its morphology. **Differential scanning calorimetry** (*DSC PerkinElmer Diamond*) was used to determine phase transitions of pure polymer and membranes prepared with different DC voltages. The samples (2-3 mg) were placed in Aluminium sample holders and heated 260-350 °C at a 5- °C/min scan

rate and then quickly cooled to room temperature with cooling rate of 100 °C/min. Second heating scan was repeated with the same input parameters.

Conductivity

The ion conductivity of AEMs was measured using a four-probe set-up (see Figure 4.2.1) by analysing Linear Galvanodynamic Sweep (LGS) curves (*AUTOLAB* Potentiostat and Booster). 1M KOH was recirculated through the system with the flow rate of 100rpm (around 8.5 ml/min for each compartment). Reference electrodes used Hg/HgO (1M NaOH)(*BASI Research products*) were connected to Lugging probes whose function is to measure voltage drop across the membrane. The current was drawn through the outer 2 probes (working electrode/anode and counter electrode/cathode), while the voltage drop was measured by inner 2 reference electrode probes across the thickness of the membrane. [40] It was important to ensure that the capillaries were always placed perpendicular and as close as possible to the membrane surface.

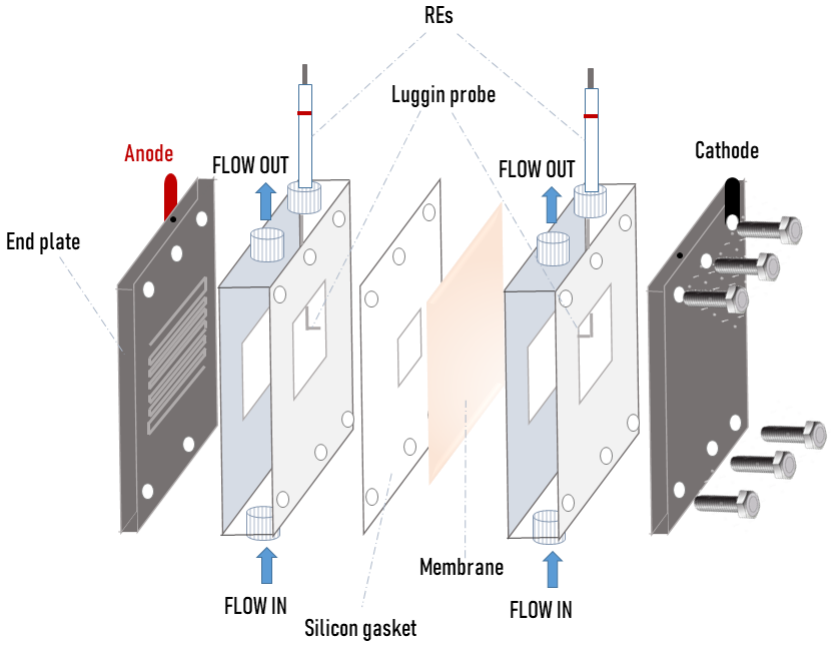

Figure 3.4: Conductivity set-up; schematic

AEMs with 5cm diameter were activated in 1M KOH for 96hr. This activation time was chosen because previous experiments demonstrated that soaking the same membrane for 96 hours resulted in the greatest reduction of the system's overpotential, compared to soaking for 48 or 72 hours (see Appendix A.2.8). Activation times above 72 hours didn't show considerable changes in the response of electrochemical system. Through-plane ion conductivity (σ) was measured at a room temperature.

The current was linearly sweeped from 0-0.8A with a scan rate of 20 mA/s and 200 mA.

Initially, LSV curves were recorded for the setup without any membrane (blank) in order to measure the Ohmic resistance of the electrolyte. The resistance of the system was calculated by the a slope of the linear current-voltage curve. Operating in the low current regime avoids bubble formation, which benefits the accuracy of the experiment. Following, the membrane was introduced and another LGS curve was measured to obtain the total resistance of the membrane and electrolyte.

Then, the resistance of the membrane was simply calculated by deducting the resistance of the blank from the total resistance.

$$R_{membrane} = R_{total} - R_{blank} \tag{3.5}$$

The ion conductivity was calculated from the equation given below:

$$\sigma[mS/cm] = \frac{d}{R_{membrane} A_{membrane}} \tag{3.6}$$

Here, $d[cm]$ is thickness of the wet membrane, measured with micrometer caliper, $R_{membrane}[\Omega]$ is the resistance of the membrane as calculated by equation 3.5, and $A_{membrane}[cm^2]$ is the surface area of the membrane that is subjected to hydroxide ion conduction. [13] The silicon gasket window was square shaped with a surface area of $A_{membrane} = 7.62cm^2$.

Ionic exchange capacity (IEC)

The ion exchange capacity (IEC) of the membranes was measured by titration using a digital titrator by *HACH*, see Figure 3.5. Firstly, pieces of similar weight (3-5 mg) were cut and dried overnight in the vacuum oven at 40 °C. Following this, the dry mass of the samples was measured with a high precision lab scale.

The membranes were then soaked for 48 hr in 40 ml 1M $NaCL$ solution to exchange Cl^- with I^- ions in the piperidinium functional groups. After required soaking period, $NaCL$ solution at the membrane surface was removed using deionized water (DI). The sample was then immersed in 40 ml 1M $NaNO_3$ for the same duration as in the first step. This solution was titrated using Chloride indicator and 0.2256 $\pm$ 0.0010N $AgNO_3$ titration catridge to determine the quantity of Cl^- ions that were exchanged back to the solution (see Figure 3.5). Solution changed colours from bright yellow to red/brown (see Appendix A.2.7). To improve the accuracy of the results, three titration readings were recorded for each titration. Using the manual provided by *HACH*, conversion equations 3.7 were used to calculate IEC. General formula is given in equation 3.7.

$$IEC[meq/g] = \frac{V_{AgNO_3} C_{AgNO_3}}{m_{dry}} \tag{3.7}$$

Here, V_{AgNO_3}, C_{AgNO_3} and m_{dry} represent volume, concentration of $AgNO_3$ and mass of dry membrane sample in gr.

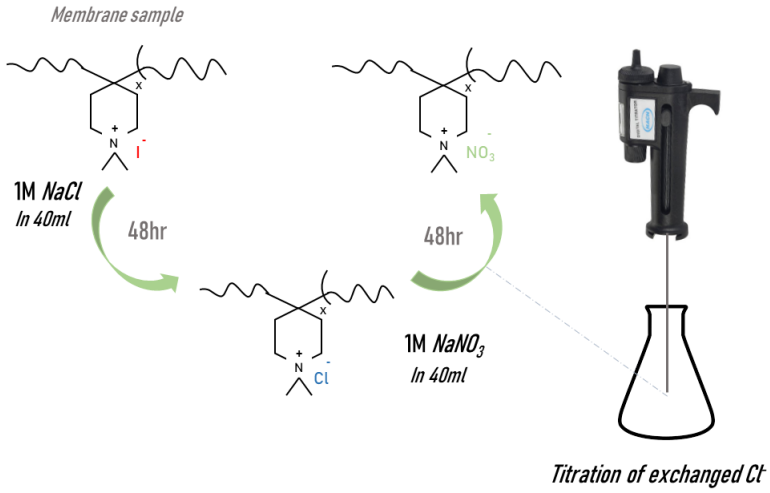

Figure 3.5: IEC schematic

3.3.2. Polymer Structural Transformations/Degradation

Fourier-transform infrared spectroscopy (FTIR)

During the FT-IR experiments with a *ThermoScientific Nicolet iS50* device, dry membranes were placed in between IR source and detector and measured using transmission mode between 500 and 4000 cm^-1. Background measurements were taken with a blank test and subtracted from the data.

Proton nuclear magnetic resonance (H NMR)

H-NMR samples were prepared by dissolving few mg of membrane samples in 0.75ml deuterated d6-DMSO (*Sigma Aldrich*, purity ≥99.9%). Literature suggests that chemical shift of d6-DMSO is 2.50ppm.[13] Furthermore, 20 μL of trifluoroacetic acid (*Sigma Aldrich*, purity ≥99.0%) was added to eliminate water peak at 3.34 ppm. The chemical structure of samples was evaluated from the spectra obtained by walk-in 400MHz *Agilent* NMR.

Small-angle X-ray scattering (SAXS)/ Wide-angle X-ray scattering (WAXS)
Wide-angle X-ray scattering (WAXS) and small-angle X-ray scattering (SAXS) were conducted at the European Synchrotron Radiation Facility (ESRF, Grenoble France) with ID31 - High Energy Beamline For Buried Interface Structure And Materials Processing. The sample-detector distance in the SAXS setup was approximately 6 meters, while for WAXS it was 50-90cm. The beam energy was 75 keV (dE = 0.1% and beamsize 3x5 μm^2). The sample was scanned at multiple positions (30), whereas results presented in the report belong to the position which showed the least noise. The scattering vector $q[nm^{-1}]$ is defined as:

$$q = \frac{4\pi}{\Lambda sin(\theta)} \tag{3.8}$$

where θ is scattering angle and λ is a wavelength of the X-ray.[41]

X-ray Photoelectron Spectroscopy (XPS)
X-ray Photoelectron Spectroscopy (XPS) measurements were conducted on solid membrane samples to analyze their elemental distribution. The measurements were performed with *K-Alpha Surface Analysis by Thermo SCIENTIFIC*, using a monochromatic source. Measurement involved collecting high-resolution spectra for key elements, primarily nitrogen, allowing for a detailed analysis of the oxidation states present in the membranes.

3.3.3. Electrochemical performance in zero gap flow cell

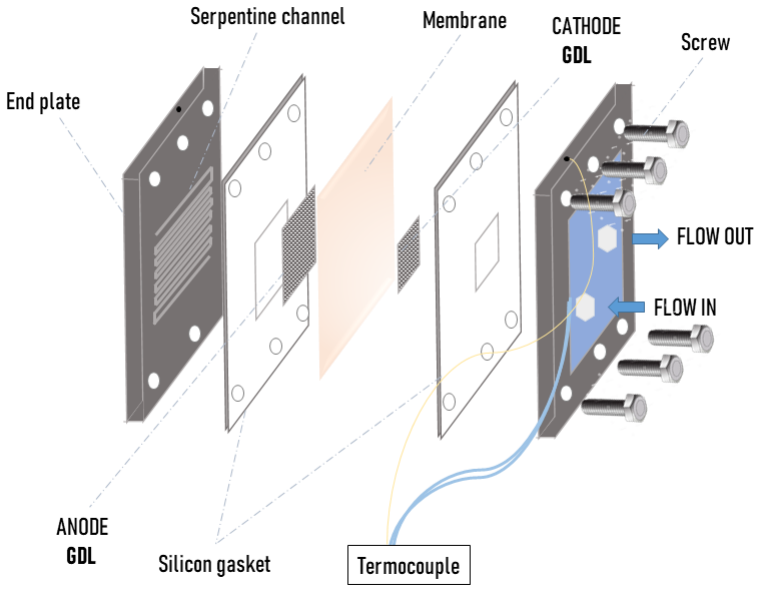

Figure 3.6: Zero gap flow cell; schematic

Electrochemical experiments were carried out in a zero-gap alkaline electrolytic cell with 1M KOH. A schematic of the cell is showed in figure 3.6.

An AEMWE cell consists of two corrosion-resistant end plates with serpentine channels (*Dioxide materials, USA*), silicon gaskets and a membrane electrode assembling (MEA). End plates are connected to the inlet and outlet flow channels for recirculation of electrolyte. Generally, MEA consists of cathode, anode and the AEM. The electrodes usually consist of a gas diffusion layer (GDL) and a catalyst layer. To simplify the process and avoid contamination of membranes with catalysts, the electrochemical experiments in this research were conducted only using pure Ni felt GDLs for both cathode and anode.

Activated membranes (5 cm diameter) were tested using given testing bench (see Figure 3.7); electrolyte was pumped through both compartments of the electrochemical cell with the flow rate of around 60 rpm (5 ml/min per each compartment). Output flows were collected and mixed in sealed bottles

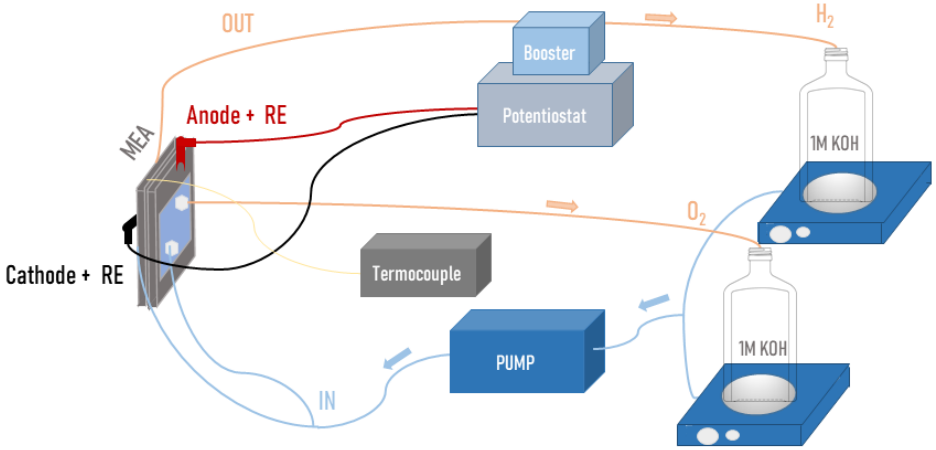

Figure 3.7: AEMWE System diagram

for supply and storage of the electrolyte. Power supply was provided by *AUTOLAB* potentiostat and booster.

Experiments were conducted at room temperature (20 ° C) and at 60 °C. Electrochemical cell temperature was stabilized using a thermocouple, while the electrolyte was heated on the heating plates.

The protocol for the electrochemical experiments is given in Table 3.1. Initially, chronopotentiometry (CP) was performed to stabilize the system. Subsequently, five scans of cyclic voltammetry (CV) experiments were conducted. Finally, CP was measured for 1500s.

Number	Experiment	Protocol
1	CP	current = 1.5 A duration = 1500 s
2	CV	voltage = 1.3-2.3 V scan rate = 20 mV/s step = 2.44 mV
3	CP	current = 1.5 A duration = 1500 s

Table 3.1: Protocol for electrochemical experiments

4

Results and Discussion

4.1. Polymer characterization ; confidential

4.1.1. Molecular weight

The molecular weight of the polymer is typically determined using Gel Permeation Chromatography (GPC). This method records the elution times of polymer chains of varying lengths as they pass through the column (stationary phase), providing values for average polymer molecular weight (Number average molar mass (M_n) and Mass average molar mass M_w). [42] However, initial measurements with GPC showed results which were very inconsistent and didn't align with anticipated outcome based on theoretical knowledge from polymer science (very low values for molecular weight and polydispersity index close to 1). Potential issues with GPC measurements might be the absence of appropriate calibration standard, strong adsorption of the charged polymer to the stationary phase and poor solubility of the polymer in DMF. [43] For figures and further explanations of obstacles encountered during the experiments, please refer to Appendix A.2.1

Considering the GPC results, the decision was made to use intrinsic viscosity as an indicator of the polymer's molecular weight, as this method has been widely used in various literature sources. [43, 44]

Intrinsic viscosity is related to viscosity-average molar mass (M_v) through Mark-Houwink-Sakurada equation, see Equation 4.1. [45]

$$[\eta] = KM^a \tag{4.1}$$

Here, K and a are Mark-Houwink parameters and are dependant on the polymer-solvent system and temperature. The polymer used in this research is novel, therefore no standard data basis can provide values for K and a, which implies that calculation of an absolute value for M_v was not possible.

To determine the Mark-Houwink parameters, multiple experiments using GPC need to be conducted with different molecular weights (MW) of the same polymer, while simultaneously measuring intrinsic viscosity. After obtaining the data, a calibration curve is constructed based on the Mark-Houwink equation. The parameters are then determined from the slope and intercept of $log[\eta]$-$logM$ curve. [45]

The viscosity of very diluted solutions (concentrations 0.25-4wt%) exhibited a linear dependency (correlation coefficient = 0.9986) with respect to the solution concentration, see Figure 4.1a. This indicates that the measurement was conducted in the dilute regime, where individual polymer chains do not interact with each other, which is necessary to determine $[\eta]$ (the viscosity of an "infinitely" diluted solution). [38]

Finally, intrinsic viscosity $[\eta]$ is calculated by the intercept of the extrapolated graph in Figure 4.1b. Polymer dissolved in DMSO gave $[\eta]$ = 0.7 dl/g. According to the literature, this indicates that the polymer has a **medium molecular weight**. [13, 44]

Cast membranes' properties depend on molecular weight; it has been shown that polymer with high $[\eta]$ provides excellent film-forming properties while polymer exhibiting low $[\eta]$ result in limited film-forming properties. [13] The polymer discussed in this report is expected to possess good film-forming properties, which will be demonstrated in the following sections.

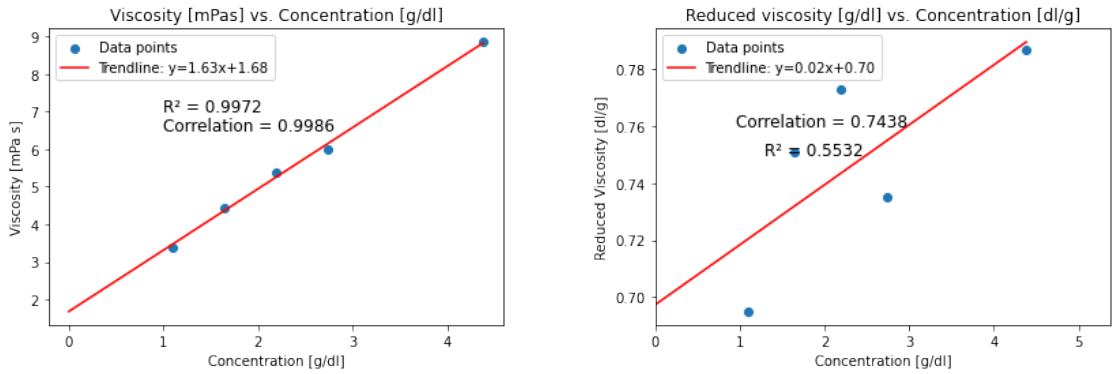

(a) Rheometry **(b)** Reduced Viscosity

Figure 4.1: Rheometry measurements

4.1.2. Glass transition temperature

DSC was used to determine the glass transition temperature of the polymer. After the experiment with the polymer solution in DMSO, peak corresponding to second-order phase transitions appeared within the temperature range between 294 and 296 °C. The glass transition temperature is a material property that indicates the temperature at which an amorphous polymer transitions from a glassy (rigid) to a rubbery state and vice versa.

T_g plays a crucial role in polymer processing. While it may not significantly impact casting at room temperature, it is important in post-treatment of membranes in electrospinning. This topic will be further discussed in the Outlook section 6.0.3.

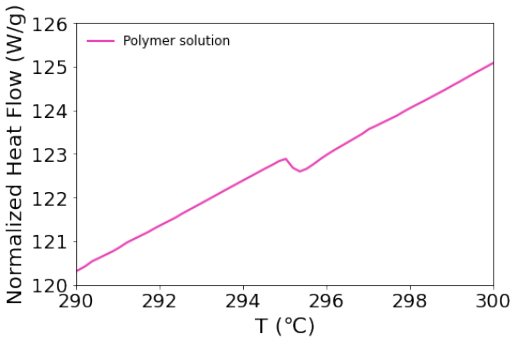

Figure 4.2: DSC - glass transition temperature

4.2. Membrane characterization

The cast membranes appeared transparent with uniform thicknesses in the central areas of the cast sheet ($30 \pm 5\ \mu m$). The edges of the membranes appeared thinner, and at higher DC voltages (above $2V$), the membranes changed color from transparent to brown/yellow. This color change might result from potential redox reactions within the polymer or solvent; however, this has not been conclusively determined in this phase of the study (for pictures please refer to Appendix A.1).

4.2.1. Conductivity and Ion Exchange capacity

Conductivity measurements at room temperature for the entire range of DC voltages, including those for Sustainion and the commercial membrane supplied by the industrial collaborator, are presented in Figure 4.3.

In all AEMs, an IEC greater than 1.5 $mmol/g$ is necessary to achieve conductivities comparable to those of PEMs (greater than 200 mS/cm at 80 $°C$) for commercial applications. [46, 47]

The trends in conductivity and IEC suggest several underlying factors that require further investigation through additional measurements. Initially, the increase in conductivity at 0.6V and 0.8V might be related to the alignment of polymer chains at the nano scale. Compared to random entanglement, oriented ion channels offer shorter hydroxide transport distance through membrane and improve utilization of cationic exchange centers, consequently increasing conductivity. [48] Based on Grotthuss and vehicle mechanisms of ion transport, hydroxide ions can more easily move through ionic channels which are lined with the polymer's functional groups. [32]
Alignment of charged polymer chains is expected with application of DC electric field and was observed in multiple literature sources. [31, 32, 49] Subsequently, the conductivity decreases (>0.8V), which could be due to a deformation of alignment in the polymer structure. [49]
Finally, there is an increase in conductivity together with IEC (above 1.8V), possibly indicating a change in the polymer's chemical structure. After 2V DC voltage, both conductivity and IEC showed moderate decline, indicating the collapse of the mentioned alignment.

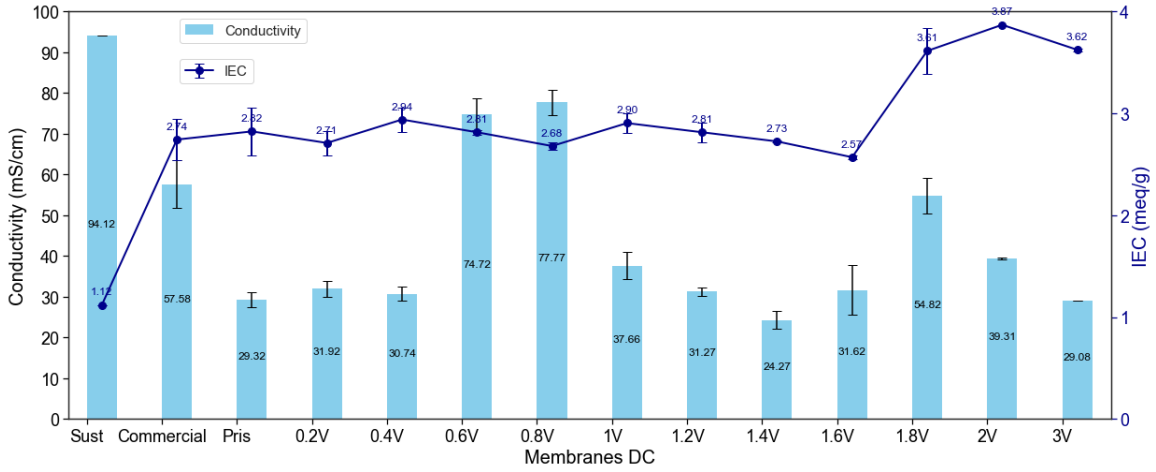

Figure 4.3: Conductivity and IEC of commercial and cast membranes

The IEC remains relatively constant for DC voltages up to 1.6V, but as said, it suddenly increases, suggesting a possible structural change in the polymer.
Notably, the most significant areas of interest are at 0.6V, 0.8V, and beyond 1.8V.
Some literature sources suggest that under very strong electric field, quaternary ammonium groups can be converted to tertiary amine groups, indicating degradation of the cationic centers and decrease in IEC. [50] The range of applied DC voltages in this study does not conclusively determine the threshold at which this degradation might occur, but at 3 V, the slight decrease in IEC could potentially happen due to this effect. Bigger degradation effects are most probably visible at higher values of DC voltages.

These observations need confirmation through other measurements, presented in following sections, to fully understand the occurring mechanisms .

4.3. Polymer Structural Transformations/Degradation

4.3.1. FTIR

Figure 4.3.1 displays close-up FTIR spectrum from 2600-1600 cm^-1 clearly showing additional peaks between 2400-2200 cm^-1 for membranes exposed to the highest DC voltage (above 1.8V).

The company involved in the project synthesised the polymer and reported that methylation time was sufficient for the quaternarization of the majority of nitrogen in piperidinium groups. Therefore, it is evident that there is a presence of tertiary nitrogen in the polymer.

DMSO used during casting is highly hygroscopic and its pH is mildly acidic (pH=6-7). [51] Undoubtedly, during casting, higher values of DC electric field cause water splitting reaction between casting blade (anode) and the casting plate (cathode). [49] With application of higher values of DC electric field in slightly acidic environment, rate of water splitting reaction increases and consequently, more protons

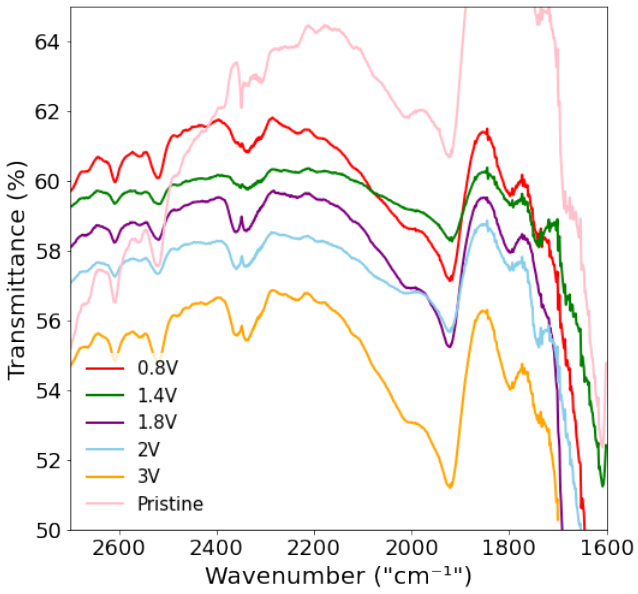

Figure 4.4: FTIR spectra

at the anode surface (casting blade) are being produced in the same intervals of time. These protons, travelling from anode (blade) to cathode (plate), could attach to pair of electrons on tertiary nitrogen, and consequently form the additional NH^+ conduction sites.

Indeed, literature sources suggest that peak stretches between 2700-2300 cm^-1 could belong to protonated tertiary nitrogen (NH^+). [52, 53] Peaks for tertiary amine salts have unique size, width and position, with no possibility of overlapping with other stretching bands in this region. [52]

Appearance of peaks in FTIR above 1.8 V could explain and confirm the increase of IEC in the same range. Protonation of tertiary nitrogen leads to activation of more cationic centers which contributes to the higher ion exchange capacity (see figure 4.3).

Protonation of tertirary nitrogen would imply change in oxidation state of nitrogen, which could ideally be detected with XPS (X-ray photoelectron spectroscopy) measurement. XPS measurements were conducted on several samples. However, due to the use of different batches during the synthesis of these samples and inconsistent information regarding methylation times, this data will be included in the Appendix A.2.5 for completeness.

In Section 4.2.1, it was mentioned that at very high DC electric fields, quaternary ammonium groups could degrade to tertiary amines. FTIR analysis would struggle to detect the presence of NH groups, as these signals are typically weak and tend to overlap with other stretching bands. [52]

4.3.2. NMR

The H NMR spectra were used to observe possible changes in the chemical structure of fabricated membranes under different DC voltages. Analysis was done for all the synthesised samples, whereas only extremes are shown in the Figure 4.5. Depicted spectra doesn't show any new peaks or peak shifts which could indicate that there is no change in chemical structure of the polymer at higher DC voltages. However, hypotheses explained in section 4.3.1 indicates protonation of tertiary Nitrogen atoms present in the polymer. Literature suggests that newly appeared NH^+ peak would be hardly detectable due to low exchange rate of the proton and piperidinium Nitrogen nuclei. [54] Furthermore, amount of tertiary Nitrogen atoms is not that high according to reported methylation time provided by the industrial collaborator. This also clarifies why detecting protonated NH^+ peaks can be challenging; low concentration of these protons within the sample leads to very weak peak intensities.

Increasing the temperature can speed up the proton exchange rate of the NH^+ group, allowing the appearance of clearer NH^+ peak.[54] However, FTIR is sufficient indicator that at higher DC voltages there is a change in chemical structure in piperidinium groups.

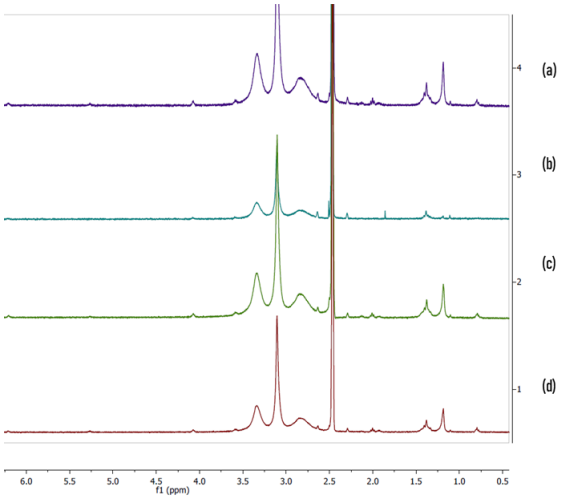

Figure 4.5: H NMR spectra of (a) pristine, (b) 3V, (c) 2V, (d) 1V

4.3.3. TGA

Thermo-gravimetric analysis was performed on membrane samples, including both pristine membranes and those subjected to a DC electric field above 0.8 V, see Figure 4.6. Results obtained suggest that the first weight decrease (25-30 % loss from 200-350 °C) relates to decomposition of piperidinum groups, whereas final weight loss can be attributed to the decomposition of the aryl backbone (70-75% above 400 °C). [13] The presented TGA curves indicate approximately 10% weight loss ascribed to the removal of the absorbed water.

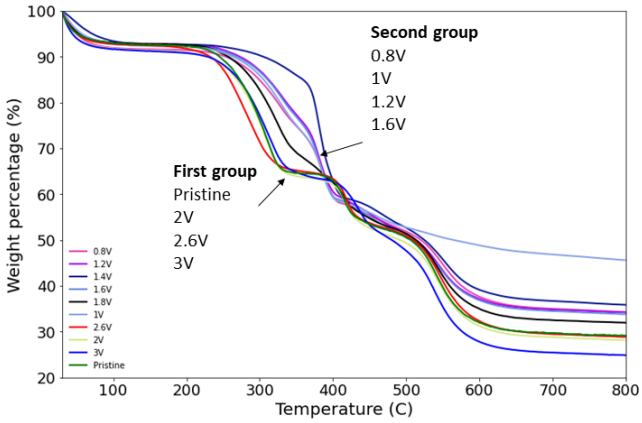

Figure 4.6: TGA profiles for different DC voltage membranes

While the overall trend in membrane decomposition appeared similar, Figure 4.6 revealed that pristine membranes and those exposed to higher ranges of DC electric fields grouped together, showing identical shape in their TGA curves (group 1). Contrary, membranes subjected to lower DC voltages displayed TGA curves of a slightly different shape (group 2).

By analysing DTG curves (see Figure 4.7b), which indicate the rate of weight loss, it was concluded that the first peak associated to the decomposition of piperidinium groups shifts to the higher temperature for the membranes from the first group. Membranes with lower DC voltage, showed decomposition of nitrogen groups at slightly higher temperatures, indicating the slower degradation, possibly due to higher alignment of polymer chains inside the membrane.The curves shown in (a) and (b) of Figure 4.7 represent averaged data for samples categorized into one of two groups.

This supports the hypothesis from Section 4.2.1. At lower voltages, the primary factor affecting con-

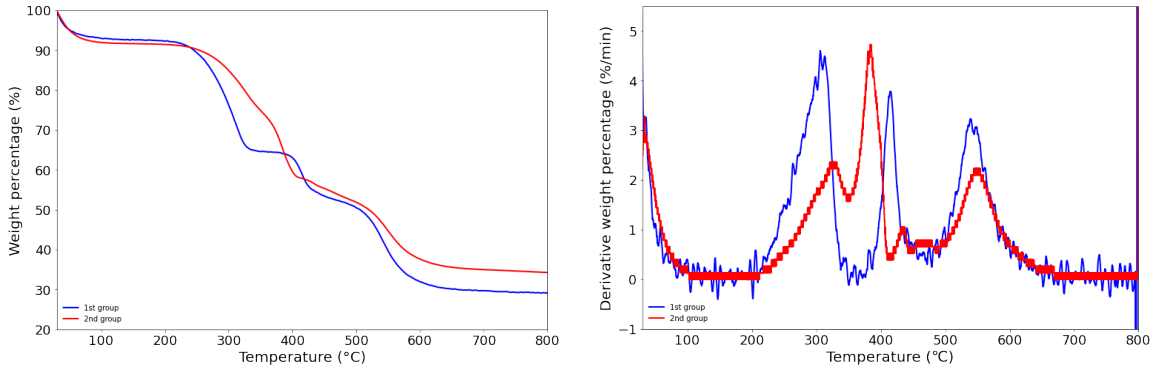

(a) Averaged TGA curves

(b) DTG curves

Figure 4.7: Comparison of thermal decomposition profiles for similarly behaved membranes as observed in TGA analysis

ductivity is the alignment of the polymer structure, leading to the decomposition of piperidinium groups at higher temperatures. However, at voltages above $2V$, piperidinium groups degrade at lower temperatures, indicating a collapse in the aligned structure.

Literature sources suggested that correlation between degree of alignment and degradation temperature is valid. Regular arrangement of polymer chains makes the membrane more resistant to thermal stresses. Aligned regions can behave as barriers for diffusion of heat and can prevent thermal energy that causes decomposition of the polymer. [30]

4.3.4. SAXS/WAXS

Depending on the volume fraction of block units, block copolymers tend to spontaneously self-assemble into various shapes such as spheres, cylinders, bicontinuous structures, lamellae, and vesicles, which lead to micro-phase separations beneficial for different applications. [55] Under the application of an electric field, charged block copolymers can be further manipulated and alligned into crystalline structures, observable at larger length scales.[56]

SAXS and WAXS measurements were employed to investigate changes in membrane morphology when exposed to a DC electric field. These two measurements together can reveal repeating structural features of polymer morphology ranging from 0.1 nm to 0.1 μm. [57]

Absolute intensities were normalized from 0 to 1 for better comparison of peak areas of obtained spectra, see Figure 4.8b. Absolute intensities include information about the sample thicknesses which were not uniform throughout experiments. Therefore, normalization was performed by dividing each spectrum by its maximum absolute intensity value, bringing all values between 0 and 1.

All samples were tested, but only the extreme ends of the DC voltage range were showed, together with the sample at $0.8V$ exhibiting the highest conductivity.

The X-axis, q, represents the scattering vector, which is connected to the scattering angle (θ) and wavelength of X-Rays (λ) with Formula 4.2.

$$q = \frac{4\pi sin\theta}{\lambda} \tag{4.2}$$

By combining this expression with Bragg's law, it is possible to interpret values on the axis through real space distance between crystal lattices, see Equation 4.3:

$$d = \frac{2\pi}{q} \tag{4.3}$$

Therefore, higher values of q, characteristic of WAXS, correspond to smaller length scales, while lower q values, typical of SAXS, provide lower resolution in observing morphology. SAXS and WAXS were done simultaneously by changing the distance of the detector from the sample holder to measure small and wide angle scattered waves, respectively.

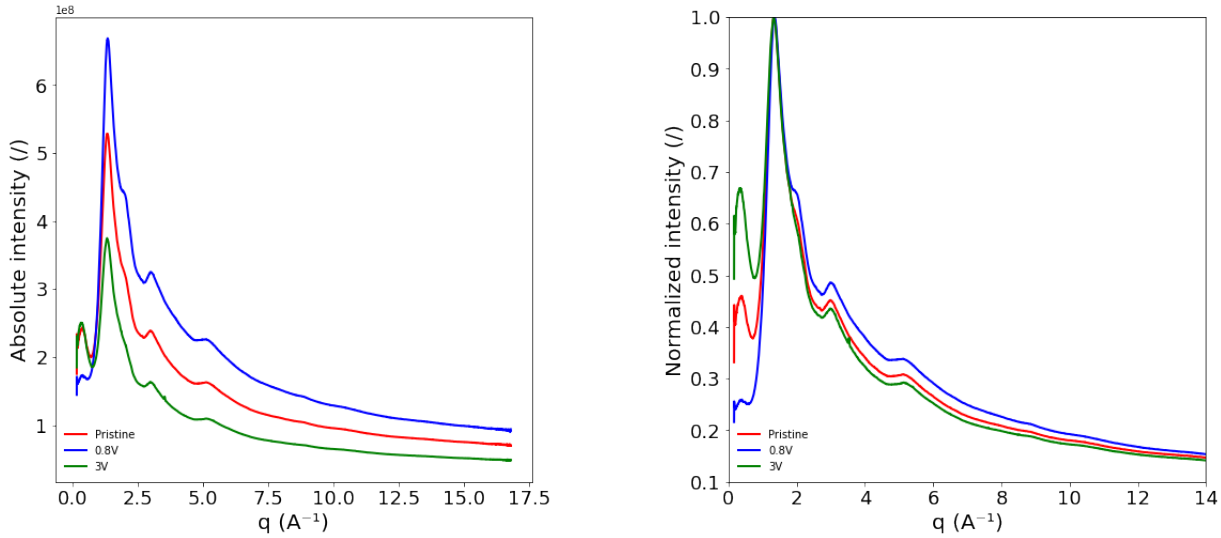

(a) WAXS spectra with absolute intensities

(b) WAXS spectra with normalized intensities

Figure 4.8: Comparison of WAXS spectra

SAXS spectra doesn't show distinguished peaks in range from of $q = 0 - 0.7\ A^{-1}$ for all dry samples (see Appendix A.2.6). This is an indication that there was no aligned structure in the lattice spacing in range up 100 nm . [58]

WAXS was performed in the q range between 0-14 $^{-1}$ to investigate the structure at molecular length scales (up to 10 nm real distance) and to determine the presence of crystalline regions in the membrane, see (b) Figure 4.8.

In literature, crystalline peaks in WAXS are often denoted with reflection (Miller) indices. However, without knowing the unit cell dimensions for the polymer provided, it is not possible to assign specific Miller indices to the peaks. Therefore, the analysis of WAXS spectra for this polymer will be conducted only qualitatively. [57]
Peaks at 0.6 A^{-1} correspond to real distance of 10.6 A, which is found to be a distance between self-assembled polymer domains. This arrangement has been observed for planar conjugated polymer systems, like one presented here. [59]

One big peak is distinguished at 2 A^{-1} which corresponds to the 3.2 A in the real space.
This prominent "ionomer" peak, typically recognizable for block copolymers, corresponds to the periodic arrangement of charged clusters within the polymer matrix. [48] It is an indication of microphase-separated structure, where the ionic groups aggregate into specific domains.
Slight shoulder on the first peak can be noticed around 2.05 A^{-1} which can be interpreted as crystalline structure formation. [60] In fact, this shoulder peak is only observed for the $0.8V$ membrane, which exhibits the highest conductivity and is expected to have the highest degree of alignment.
Intensity of normalized peaks for $0.8V$ indicate higher level of crystallinity and tighter packing of the polymer chains. [48, 59]
Peaks emerging at $q = 3A^{-1}$ and $q = 5A^{-1}$ arise from block copolymer alignment on the 0.1 nm length scale. Due to the lack of literature on polymers with similar functional groups, identifying the specific type of polymer alignment is not possible. However, higher peak intensities for the 0.8V sample, compared to the pristine membrane, suggest a greater degree of polymer chain order, which explains the higher ionic conductivity at this DC voltage. Contrary, lower peak intensities for $3V$ relative to the pristine membrane prove collapsing of the aligned structure at higher applied DC voltages.

4.3.5. Water Uptake Ratio

Soaked membranes in solution swell, causing the change in the thickness compared to dry state. When in contact with liquid, the volume of polymer expands due to spreading of solvent molecules within the

structure. Swelling ratio is dependant on the temperature and operating pressure of the electrochemical cell, as well as the degree of cross-linking between the polymer chains.[48] The degree of swelling heavily depends on the chemical structure of the polymer, specially on the presence of hydrophilic charged groups. [13] Polymers with relatively high presence of ionic centers possess high IEC, and simultaneously enhance ion transportation. However, very high IEC leads to high swelling, reduced permselectivity, mechanical deterioration of membranes and degradation of the catalyst layer. [5, 23, 58] Furthermore, excess of swelling can lead to decrease in conducting ion concentration and result in poor conductivity. [20] As mentioned, membranes cast with the employment of a DC electric field exhibit polymer chain rearrangement into ionic channels, which, according to the literature, leads to increased swelling ratios. [5]

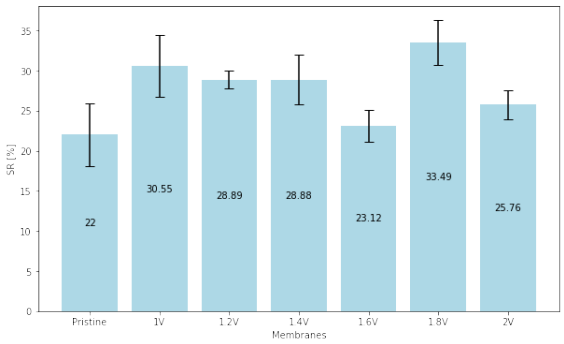

Figure 4.9: Water Upatake ratio for membranes samples above $1V$ DC

Membranes above $1V$ DC voltage, behave accordingly to expected trends, see Figure 4.9. Pristine membrane shows minimum water swelling ratio, whereas membranes cast with applied DC electric field show slight increase, due to rearrangement of polymer chains, proved by WAXS. Maximum water swelling ratio is achieved at 1.8 V where IEC is shown to be the highest due to formation of additional charged sites proved by FTIR.

Overall, the water swelling ratio is a straightforward measurement that supports the points discussed in the previous sections. It shows that the polymer's swelling falls between 20-40%, similar with most available AEMs. [23]

4.4. Electrochemical performance in zero gap flow cell

Simple electrochemical experiments using a GDL without a catalyst were conducted to confirm the observed trends in conductivity and IEC. Due to a limited supply of polymer, it was only possible to cast samples once or twice which is why they exhibited variations in thicknesses.
Since membrane thickness significantly affects transport resistance and the voltage and current output in electrochemical experiments, the membranes were categorized into two groups for better comparability, as shown in Table 4.1.

Membrane	Wet Thickness (µm)
1V	61
1.2V	65
2V	65
Pristine	48
1.6V	50
1.8V	51
3V	51.5

Table 4.1: Grouping of membranes with similar thicknesses

This section of the thesis focuses on the characterization of membranes subjected to higher DC voltages (above $1V$). Chronopotentiometry experiments showed stable cell voltage during application of constant 1.5 A current for 1500 s, see Appendix A.2.8. The stable potential at the anode depends on the electrode's properties (Ni GDL) and the current applied. Small differences in potentials for all membranes suggest variations in membrane resistances for different samples.

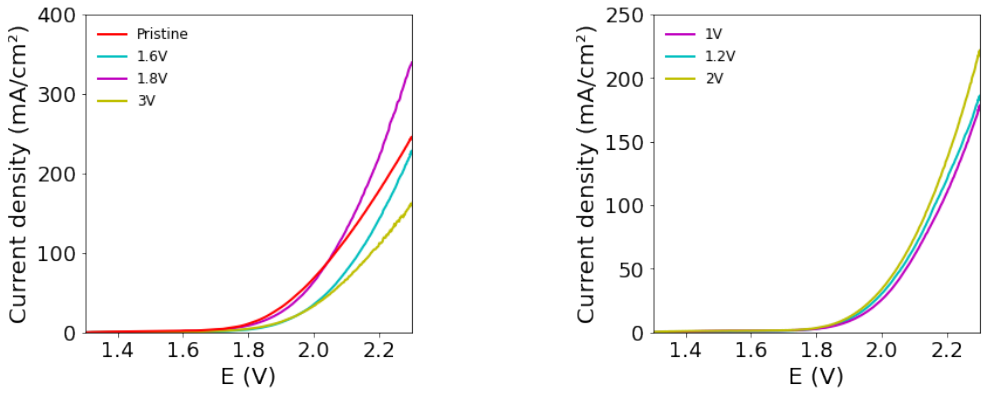

(a) Polarisation curves room T 50 $\pm 2\mu m$

(b) Polarisation curves room T 60 $\pm 4\mu m$

Figure 4.10: Comparison of polarisation curves at room temperature

On the other hand, CVs in Figure 4.10 indicate that higher current densities are achieved for membranes with higher values for conductivity. Figure 4.10a, illustrates that the membrane sample with applied 1.8 V DC voltage exhibits the highest current densities over the range of applied potentials. This is consistent with previous observations and suggests that this membrane has the lowest resistance. Confirmation for this could also come from observing offset potentials at which current starts to flow through the circuit; for 1.8 V membrane, this potential is the lowest, indicating the lowest system overpotentials due to increased conductivity of the membrane. [61] Similar trend was observed at the elevated temperatures with output current densities much higher, due to increased reaction rate constants of the reactions happening in the system. Variations in expected trends can be assigned to slight temperature differences in the system during different experiments. Furthermore, more rigorous electrochemical experiments suggest use of torque for applying constant compression on the zero gap flow cell. This parameter could affect the current output and needs to be optimized in future for precise and strict evaluation of membrane electrochemical performance. [62]

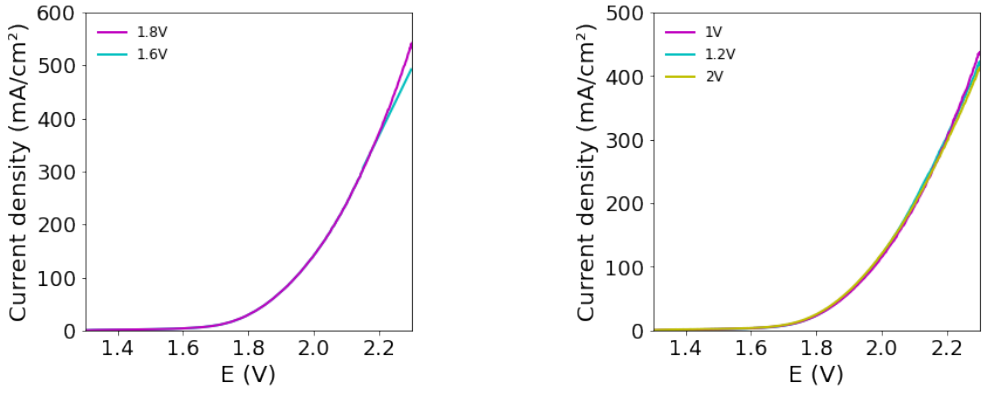

(a) Polarisation curves elevated T 50 $\pm 2\mu m$

(b) Polarisation curves elevated T 60 $\pm 4\mu m$

Figure 4.11: Comparison of Polarisation curves at 60 $^{\circ}C$ measurements

5

Conclusion

In this study, we successfully synthesized and characterized anion exchange membranes with the application of a DC electric field during casting. Hydroxide conductivity and IEC measurements indicated different trends within the 0-3V range of applied DC electric field. As the DC voltage increased, higher alignment of polymeric chains was expected due to reorientation of poly-electrolyte in dielectric solvent. This phenomenon was proved by WAXS spectra which revealed emerging crystalline structures in membranes showing the highest conductivity. Additionally, TGA analysis indicated that membranes demonstrating higher conductivity decomposed at slower rates, suggesting a more ordered structural arrangement. Membranes cast with 0.6 V and 0.8 V exhibited the most promising conductivity values at room temperature, nearly comparable to commercially available products.
On the other hand, DC electric field above $1.8V$ indicated considerable increase in IEC. FTIR analysis proved our hypothesis; above $1.8V$ there was an emerging peak between 2400-2200 cm^{-1} suggesting presence of tertiary amine salts. XPS analysis indicated the existence of both oxidation states of nitrogen. However, additional investigation and ensuring consistency in sample preparation are necessary to validate and integrate these results into the discussion.

Electrochemical tests confirmed the conductivity trend: membranes with higher conductivity exhibited greater current density due to lower resistance.

Applying DC electric field during membrane casting promises to be attractive method for enhancing membranes' properties. This study proves increasing trend of conductivity at certain ranges of DC voltage applied alongside chemical structure change. However more thorough investigation on mechanical stability and durability of the membranes should be conducted to conclude whether newly synthesized membranes are competitive to commercially available products.

6 Outlook

This project successfully synthesized and characterized membranes in wide range of applied DC voltages with enhanced properties compared to the pristine sample.
Experimental work has managed to qualitatively explain and prove mechanism underlying the changing trends in macroscopic properties of the membranes, such as IEC and ionic conductivity.
However, we believe that further research into the membranes' properties is beneficial for gaining fundamental understanding of polymer's behavior under the application of a DC electric field.

During the project, technical constraints such as the limited availability of the polymer represented a big obstacle to presenting a more comprehensive analysis. Unfortunately, some experiments that could have further proven the appearing trends were unable to yield suitable results due to inconsistencies in samples preparation.
These experiments will be addressed in Appendix A, as they could be valuable for further research in this area. Possible future research directions are outlined in the following sections.

6.0.1. Cast composite membranes with employment of DC electric field

Cast composite membranes represent a promising pathway for enhancing properties of polymeric membranes. The scientific community has shown increased interest in this area, with numerous studies exploring different polymer matrices and filler materials. Some of the most promising fillers are shown to be carbon nanotubes, graphene oxide and layered double hydroxides. [63] Achieving optimal loading of fillers in matrix is crucial for successful property enhancement. Moreover, surface treatment of fillers can improve filler-matrix compatibility, and enhance the membrane properties such as conductivity and durability. Some studies show that composite membranes with graphene oxide showed very small degradation rates of polymer functional groups and increased conductivities compared to pristine samples. [64] Together with electro-casting, composite fillers can yield even better performance, increasing efficiencies in AEMWE systems. In electro-casting, it's crucial to note that fillers must be non-conductive to prevent agglomeration and potential short circuits during the process.[64]

We believe this is a valuable pathway for the future research.

6.0.2. Electro-casting from heterogeneous solution

The addition of a non-solvent to the casting solution has been demonstrated as an effective method for enhancing micro-phase separation and alignment during electro-casting. The presence of a non-solvent can help in the orientation of charged polymers in presence of dielectric solvent under the influence of an electric field. Membranes produced using this approach exhibited improved through-plane conductivity compared to membranes electro-cast solely from the mother solvent. Additionally, despite phase separation occurring in the casting solution, enhanced mechanical properties were observed. [48]

6.0.3. Electrospinning

Finally, we cannot finish this report without reflecting upon the work done in the first part of the MSc project. Electrospinning has been shown as a promising fabrication technique which could enhance

charge transport behaviour due to better micro structural morphology.

Due to technical difficulties, membrane fabrication was not completed. However, optimal parameters for nanofiber fabrication were achieved. This provides a strong starting point for future research, as membranes produced using this method could potentially surpass the properties of cast membranes, according to the literature. Optimal production parameters are given below.

Polymer solution concentration: 22 wt%
Flow rate: 0.1 ml/hr
Distance between needle and collector: 20 cm
Needle diameter: 0.8 mm
ω (rotary drum speed): 500 rpm
Injected polymer solution volume: 2.1-2.2 ml
Room temperature
RH (Relative humidity): 45%
Needle position: HOME (center)
Voltage: 23 kV

Obtained jet and nanofibers pictured with microscope are shown in the Figure 6.1.

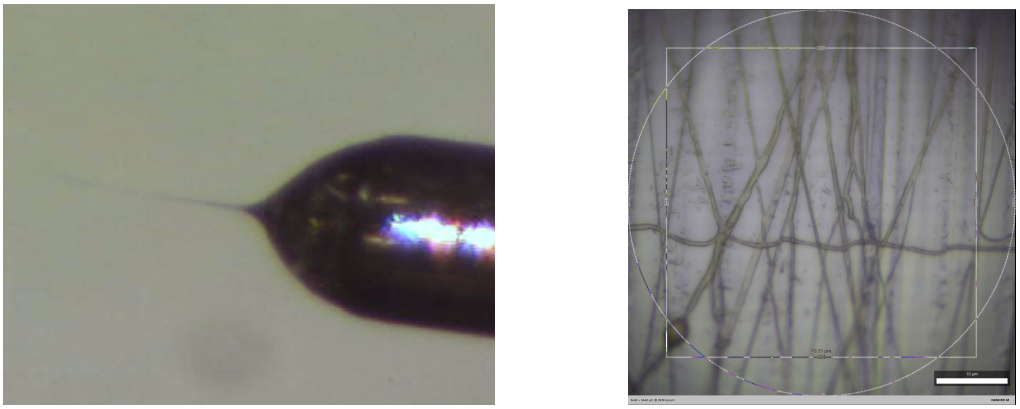

(a) Stable nanofiber jet

(b) Nanofibers detected under microscope

Figure 6.1: Optimal production process parameters for electrospinning

To proceed with this research, it is recommended to conduct a thorough examination of the nanofiber mats post-treatment. One proposed approach is to employ hot-pressing, utilizing temperatures slightly below the identified glass transition temperature. This way, morphology of the obtained nanofibers is staying intact, and better membrane performance can be expected. Pressures used during post-treatment are usually reported to be around 15 MPa. [65]

References

[1] L. Barreto et al. “Recent progress in alkaline water electrolysis for hydrogen production and applications”. In: *Progress in Energy and Combustion Science* (2009). URL: https://www.sciencedirect.com/science/article/pii/S0360128509000598.

[2] International Energy Agency. *Low Emission Fuels: Hydrogen*. 2023. URL: https://www.iea.org/energy-system/low-emission-fuels/hydrogen.

[3] Immanuel Vincent and Dmitri Bessarabov. “Low cost hydrogen production by anion exchange membrane electrolysis: A Review”. In: *Renewable and Sustainable Energy Reviews* 81 (2018), pp. 1690–1704. DOI: 10.1016/j.rser.2017.05.258.

[4] Ebrahim Abouzari-Lotf et al. “Highly conductive anion exchange membranes based on polymer networks containing imidazolium functionalised side chains”. In: *Scientific Reports* 11.1 (2021). DOI: 10.1038/s41598-021-83161-9.

[5] Jae-Hun Kim et al. “Preparation of high-conductivity QPPO (quaternary-aminated poly (2,6-dimethyl-1,4-phenyleneoxide)) membranes by electrical treatment”. In: *Journal of Membrane Science* 553 (2018), pp. 82–89. DOI: 10.1016/j.memsci.2017.12.009.

[6] Ankica Kovač, Matej Paranos, and Doria Marciuš. “Hydrogen in energy transition: A Review”. In: *International Journal of Hydrogen Energy* 46.16 (2021), pp. 10016–10035. DOI: 10.1016/j.ijhydene.2020.11.256.

[7] Nanjun Chen et al. “High-performance anion exchange membrane water electrolyzers with a current density of 7.68 a cm−2 and a durability of 1000 hours”. In: *Energy amp;amp; Environmental Science* 14.12 (2021), pp. 6338–6348. DOI: 10.1039/d1ee02642a.

[8] Asep Muhamad Samsudin et al. “Preparation and characterization of QPVA/PDDA electrospun nanofiber anion exchange membranes for alkaline fuel cells”. In: *Nanomaterials* 12.22 (2022), p. 3965. DOI: 10.3390/nano12223965.

[9] Yi-cun Zhou et al. “Electrospun modified polyketone-based anion exchange membranes with high ionic conductivity and robust mechanical properties”. In: *ACS Applied Energy Materials* 4.5 (2021), pp. 5187–5200. DOI: 10.1021/acsaem.1c00727.

[10] E. Drioli and Lidietta Giorno. *Membrane operations: Innovative separations and transformations*. Wiley-VCH, 2009.

[11] Zhihao Shang, Ryszard Wycisk, and Peter Pintauro. “Electrospun composite proton-exchange and anion-exchange membranes for fuel cells”. In: *Energies* 14.20 (2021), p. 6709. DOI: 10.3390/en14206709.

[12] URL: https://dioxidematerials.com/products/sustainion/.

[13] Nanjun Chen et al. “Poly(fluorenyl aryl piperidinium) membranes and ionomers for anion exchange membrane fuel cells”. In: *Nature Communications* 12.1 (2021). DOI: 10.1038/s41467-021-22612-3.

[14] Nanjun Chen et al. “Chemically amp; physically stable crosslinked poly(aryl-co-aryl piperidinium)s for anion exchange membrane fuel cells”. In: *Journal of Membrane Science* 638 (2021), p. 119685. DOI: 10.1016/j.memsci.2021.119685.

[15] Volodymyr Tymofiiv et al. “Hydrogen production for improved transportation system as a part of Smart Cities”. In: *Lecture Notes of the Institute for Computer Sciences, Social Informatics and Telecommunications Engineering* (2022), pp. 221–233. DOI: 10.1007/978-3-031-15101-9_16.

[16] Jae-Hun Kim et al. “Preparation of high-conductivity QPPO (quaternary-aminated poly (2,6-dimethyl-1,4-phenyleneoxide)) membranes by electrical treatment”. In: *Journal of Membrane Science* 553 (2018), pp. 82–89. DOI: 10.1016/j.memsci.2017.12.009.

[17] Hirokazu Kojima et al. “Influence of renewable energy power fluctuations on water electrolysis for green hydrogen production”. In: *International Journal of Hydrogen Energy* 48.12 (2023), pp. 4572–4593. DOI: 10.1016/j.ijhydene.2022.11.018.

[18] URL: https://www.researchgate.net/publication/338534224_Hydrogen_production_for_energy_An_overview.

[19] Iea. *Electrolysers - Energy System*. URL: https://www.iea.org/energy-system/low-emission-fuels/electrolysers.

[20] Xiuqin Wang. In: *Poly(arylene piperidinium)-based anion exchange membranes for water electrolysis* (). DOI: 10.3990/1.9789036554275.

[21] Qiucheng Xu et al. “Anion exchange membrane water electrolyzer: Electrode Design, lab-scaled testing system and performance evaluation”. In: *EnergyChem* 4.5 (2022), p. 100087. DOI: 10.1016/j.enchem.2022.100087.

[22] Naiying Du et al. “Anion-exchange membrane water electrolyzers”. In: *Chemical Reviews* 122.13 (2022), pp. 11830–11895. DOI: 10.1021/acs.chemrev.1c00854.

[23] Naiying Du et al. “Anion-exchange membrane water electrolyzers”. In: *Chemical Reviews* 122.13 (2022), pp. 11830–11895. DOI: 10.1021/acs.chemrev.1c00854.

[24] Michael A. Hickner, Andrew M. Herring, and E. Bryan Coughlin. “Anion exchange membranes: Current status and moving forward”. In: *Journal of Polymer Science Part B: Polymer Physics* 51.24 (2013), pp. 1727–1735. DOI: 10.1002/polb.23395.

[25] Eun Joo Park et al. *Membrane strategies for water electrolysis*. 2022. URL: https://www.osti.gov/servlets/purl/1889888.

[26] Bowen Yang and Zhang Cunman. “Progress in constructing high-performance anion exchange Membrane: Molecular design, microphase controllability and In-device property”. In: 457 (2023). DOI: 10.1016/j.cej.2022.141094.

[27] Tequila A.L. Harris and Daniel F. Walczyk. “Development of a casting technique for membrane material used in high-temperature PEM fuel cells”. In: *Journal of Manufacturing Processes* 8.1 (2006), pp. 8–20. DOI: 10.1016/s1526-6125(06)70097-4.

[28] Karl Amundson et al. “Corrections: Effect of an electric field on block copolymer microstructure.” In: *Macromolecules* 25.3 (1992), pp. 1200–1200. DOI: 10.1021/ma00029a605.

[29] Y Oren, V Freger, and C Linder. “Highly conductive ordered heterogeneous ion-exchange membranes”. In: *Journal of Membrane Science* 239.1 (2004), pp. 17–26. DOI: 10.1016/j.memsci.2003.12.031.

[30] Karl Amundson et al. “Corrections: Effect of an electric field on block copolymer microstructure.” In: *Macromolecules* 25.3 (1992), pp. 1200–1200. DOI: 10.1021/ma00029a605.

[31] Jae-Hun Kim et al. “Fabrication of a composite anion exchange membrane with aligned ion channels for a high-performance non-aqueous vanadium Redox Flow Battery”. In: *RSC Advances* 10.9 (2020), pp. 5010–5025. DOI: 10.1039/c9ra08616a.

[32] Seungbo Ryu et al. “Investigation of the effects of electric fields on the nanostructure of Nafion and its proton conductivity”. In: *Journal of Materials Chemistry A* 6.42 (2018), pp. 20836–20843. DOI: 10.1039/c8ta06752j.

[33] Jiefeng Pan et al. “Anion exchange membranes from hot-pressed electrospun QPPO–sio2 hybrid nanofibers for acid recovery”. In: *Journal of Membrane Science* 480 (2015), pp. 115–121. DOI: 10.1016/j.memsci.2015.01.040.

[34] Xue Gong et al. “Electrospun imidazolium functionalized multiwalled carbon nanotube/ Polysulfone Inorganic-organic nanofibers for reinforced anion exchange membranes”. In: *International Journal of Hydrogen Energy* 43.46 (2018), pp. 21547–21559. DOI: 10.1016/j.ijhydene.2018.09.210.

[35] Adnan Haider, Sajjad Haider, and Inn-Kyu Kang. “A comprehensive review summarizing the effect of electrospinning parameters and potential applications of nanofibers in biomedical and biotechnology”. In: *Arabian Journal of Chemistry* 11.8 (2018), pp. 1165–1188. DOI: 10.1016/j.arabjc.2015.11.015.

[36] Rakhi Sood et al. “Electrospun nanofibre composite polymer electrolyte fuel cell and electrolysis membranes”. In: *Nano Energy* 26 (2016), pp. 729–745. DOI: 10.1016/j.nanoen.2016.06.027.

[37] Josephat U. Izunobi and Clement L. Higginbotham. “Polymer Molecular Weight Analysis by ^{1}H NMR Spectroscopy”. In: *Journal of Chemical Education* 88.8 (2011), pp. 1098–1104. DOI: 10.1021/ed100461v.

[38] Wei Lu and Jimmy Mays. “Dilute solution viscometry of polymers”. In: *Molecular Characterization of Polymers* (2021), pp. 261–280. DOI: 10.1016/b978-0-12-819768-4.00008-7.

[39] Anton Paar. *Intrinsic viscosity determination: Anton Paar*. 2022. URL: https://wiki.anton-paar.com/en/intrinsic-viscosity-determination/.

[40] Ismailia L. Escalante-García et al. “Performance of a non-aqueous vanadium acetylacetonate prototype redox flow battery: Examination of separators and capacity decay”. In: *Journal of The Electrochemical Society* 162.3 (2014). DOI: 10.1149/2.0471503jes.

[41] Vincent Voet. “Block copolymers based on poly(vinylidene fluoride)”. English. PhD thesis. University of Groningen, 2015. ISBN: 978-90-367-7474-1.

[42] Agilent Technologies. *A Guide to Gel Permeation Chromatography and Size Exclusion Chromatography*. Tech. rep. Agilent Technologies, 2011. URL: https://www.agilent.com/cs/library/primers/Public/5990-6969EN%20GPC%20SEC%20Chrom%20Guide.pdf.

[43] Xingyu Wu et al. “Branched poly(aryl piperidinium) membranes for anion□exchange membrane fuel cells”. en. In: *Angew. Chem. Weinheim Bergstr. Ger.* 134.7 (Feb. 2022).

[44] Joel Olsson, Thanh Huong Pham, and Patric Jannasch. “Poly(arylene piperidinium) hydroxide ion exchange membranes: synthesis, alkaline stability and conductivity”. In: 28.2 (2018). DOI: 10.1002/ADFM.201702758.

[45] George Sakellariou, Aikaterini Siakali-Kioulafa, and Nikos Hadjichristidis. “Synthesis, Chain Flexibility, and Glass-Transition Temperature of Poly (2,2-Diphenylethyl Methacrylate)”. In: 8.4 (2003). DOI: 10.1080/10236660304881.

[46] Eun Joo Park and Yu Seung Kim. “Quaternized aryl ether-free polyaromatics for alkaline membrane fuel cells: synthesis, properties, and performance – a topical review”. In: 6.32 (2018). DOI: 10.1039/C8TA05428B.

[47] Michael Witt and Nur amalia daud. “High performance poly(carbazolyl aryl piperidinium) anion exchange membranes for alkaline fuel cells”. In: 657 (2022). DOI: 10.1016/j.memsci.2022.120676.

[48] Shixiong Zhao, Jiejing Zhang, and Yuxin Wang. “Electro-casting of proton exchange membranes from a heterogeneous solution”. In: 242 (2013). DOI: 10.1016/J.JPOWSOUR.2013.05.024.

[49] Ju-Young Lee et al. “Electrically aligned ion channels in cation exchange membranes and their polarized conductivity”. In: 478 (2015). DOI: 10.1016/J.MEMSCI.2014.12.049.

[50] Jae-Hwan Choi and Seung-Hyeon Moon. “Structural change of ion-exchange membrane surfaces under high electric fields and its effects on membrane properties”. In: 265.1 (2003). DOI: 10.1016/S0021-9797(03)00136-X.

[51] *Dimethyl Sulfoxide*. URL: https://pubchem.ncbi.nlm.nih.gov/compound/679.

[52] *Organic Nitrogen Compounds V: Amine Salts*. 2020. URL: https://www.spectroscopyonline.com/view/organic-nitrogen-compounds-v-amine-salts.

[53] Donald L. Pavia et al. *Introduction to Spectroscopy*. 2008.

[54] “Determination of molar ratio of primary secondary and tertiary amines in polymers by applying derivatization and NMR spectroscopy”. In: 56 (2016), pp. 174–179. DOI: 10.1016/j.polymertesting.2016.10.013. URL: https://www.sciencedirect.com/science/article/pii/S0142941816305682.

[55] Yiyong Mai and Adi Eisenberg. “Self-assembly of block copolymers”. In: 41.18 (2012). DOI: 10.1039/C2CS35115C.

[56] Yiyong Mai and Adi Eisenberg. “Self-assembly of block copolymers”. In: 41.18 (2012). DOI: 10.1039/C2CS35115C.

[57] Edward A. Nagul et al. “Nanostructural characterisation of polymer inclusion membranes using X-ray scattering”. In: 588 (2019). DOI: 10.1016/J.MEMSCI.2019.117208.

[58] “Anion Exchange Membrane Based on Interpenetrating Polymer Network with Ultrahigh Ion Conductivity and Excellent Stability for Alkaline Fuel Cell”. In: 2020 (2020), p. 4794706. DOI: 10.34133/2020/4794706. URL: https://www.ncbi.nlm.nih.gov/pmc/articles/PMC7243038/.

[59] Woo-Hyung Lee et al. “Poly(terphenylene) Anion Exchange Membranes: The Effect of Backbone Structure on Morphology and Membrane Property”. In: 6.5 (2017). DOI: 10.1021/ACSMACROLETT.7B00148.

[60] Laurent Rubatat et al. “Structural study of proton-conducting fluorous block copolymer membranes”. In: 39.2 (2006). DOI: 10.1021/MA0520139.

[61] *Cyclic Voltammetry Basic Principles, Theory Setup*. 2020. URL: https://www.ossila.com/pages/cyclic-voltammetry.

[62] Robert Phillips and Charles W. Dunnill. “Zero gap alkaline electrolysis cell design for renewable energy storage as hydrogen gas”. In: 6.102 (2016). DOI: 10.1039/C6RA22242K.

[63] Riccardo Narducci et al. “Anion Exchange Membranes with 1D, 2D and 3D Fillers: A Review”. In: 13.22 (2021). DOI: 10.3390/POLYM13223887.

[64] Nicholas Carboni et al. “Composite anion exchange membranes based on graphene oxide for water electrolyzer applications”. In: *Electrochimica Acta* 486 (2024), p. 144090. ISSN: 0013-4686. DOI: https://doi.org/10.1016/j.electacta.2024.144090. URL: https://www.sciencedirect.com/science/article/pii/S0013468624003323.

[65] Zhihao Shang, Ryszard Wycisk, and Peter N. Pintauro. “Electrospun Composite Proton-Exchange and Anion-Exchange Membranes for Fuel Cells”. In: 14.20 (2021). DOI: 10.3390/EN14206709.

[66] Robert Phillips and Charles W. Dunnill. “Zero gap alkaline electrolysis cell design for renewable energy storage as hydrogen gas”. In: 6.102 (2016). DOI: 10.1039/C6RA22242K.

[67] “X-ray Photoelectron Spectroscopy (XPS) Analysis of Nitrogen Environment in Small Extracellular Vesicle Membranes: A Potential Novel Technique with Application for Cancer Screening”. In: 15.9 (), p. 2479. DOI: 10.3390/cancers15092479. URL: https://www.ncbi.nlm.nih.gov/pmc/articles/PMC10177571/.

A

Appendix

A.1. Membrane casting

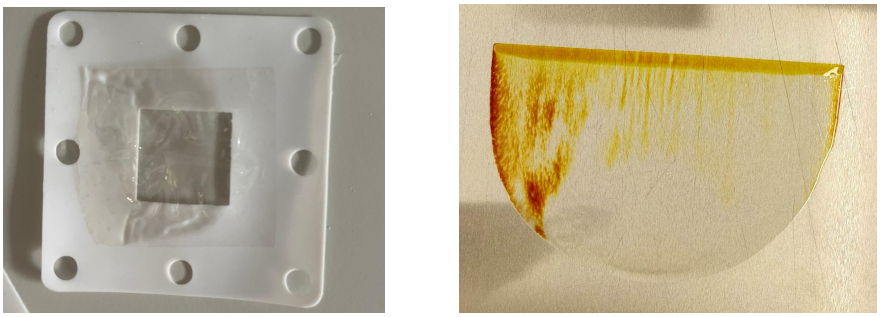

(a) Transparent activated membrane

(b) $2V$ DC electric field membrane

Figure A.1: Electro-cast membranes

A.2. Polymer characterization

A.2.1. GPC

Samples experimented with GPC showed rather low values for molecular weight of the polymer, from 3000-7500 g/mol, see Figure A.2. Polydispersity index was always around 1, which also indicated inconclusive measurements. After some thinking, possible problems were presented; (a) Polymer is not dissolved well in DMF (polymer chains are filtered out before the elution through the column), (b) Concentration of polymer solution is not suitable, (c) PEO calibration curve is not suitable, (d) Possible adsorption of cationic groups on the column. PEO calibration curve was standard in-built the system, and its suitability for our polymer couldn't be checked due to unavailable data on hydrodynamic volume of the polymer. Finally, as a most probable reason, we suspect that cationic groups were adsorbing to the column, giving very long elution times and consequently, small MW.

A.2.2. DMA

Glass-transition (Tg) temperature, storage and loss modulus of membrane samples were measured with **Dynamic Mechanical Analysis** (*DMA RSA-G2 Solids Analyzer, TA Instrument*). All membranes were cut into 2 x 1 cm samples and then fixed with tension clamps in the DMA system. Following protocol was employed for obtaining temperature ramp curves; testing was done with a pre-load force 0.01N, in 1 Hz single-frequency strain mode, and a force track of 125% under a constant nitrogen supply. Temperature ramp was done from room temperature to 450 °C with a 10 °C/min ramping rate.

DMA is a highly precise technique used to determine the glass transition temperature and mechanical properties of materials. Temperature ramp experiments using DMA at *Faculty of Aerspace Engineering, TU DELFT,* were conducted on very thin membranes with inconsistent thicknesses to confirm

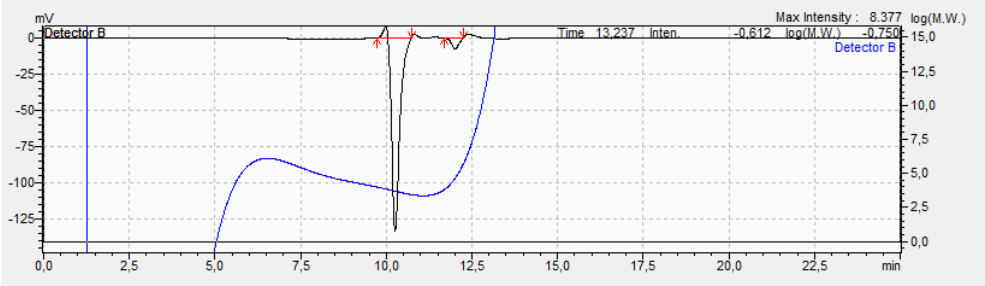

Figure A.2: GPC, polymer solution in DMF

the change in glass transition temperature for different samples discussed in section A.2.4. However, the expected profiles for storage modulus, loss modulus, and tan(δ) as a function of temperature were not obtained because membranes slipping between the tensile clamps. Mechanical properties were not analyzed, as it was estimated that the small tensile strength (TS) and elongation at break (EB) could damage the delicate equipment. Obtained profiles are shown in Figure A.3. Out of many measurements, the ones presented here were the only ones that consistently showed similar results. However, they still indicated a very low glass transition temperature, around 200 °C, compared to obtained DSC analysis. For more accurate measurements, it is recommended to prepare slightly thicker samples, around 70 μm.

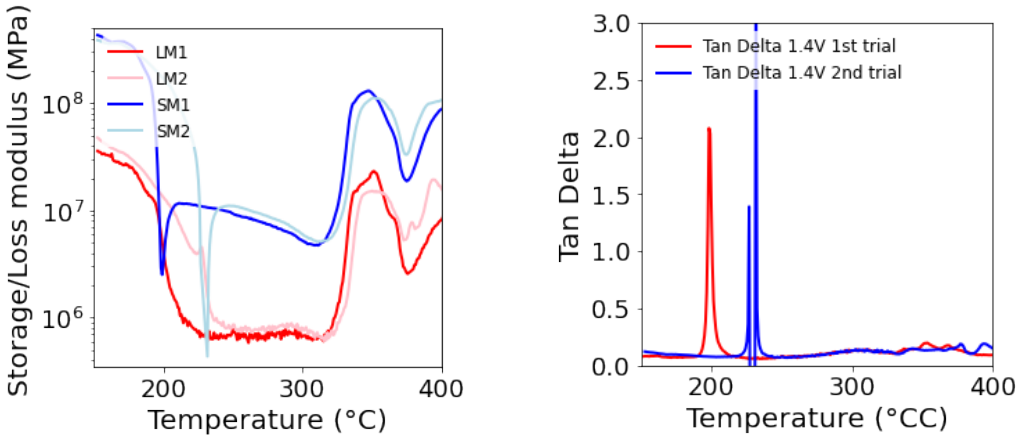

(a) Storage and Loss Modulus vs. T [°C]

(b) Tan δ vs. T [°C]

Figure A.3: DMA; Temperature Ramp Analysis

A.2.3. UTM

The UTM (Universal Testing Machine) at the *Faculty of Aerospace Engineering* was used for mechanical characterization to obtain stress-strain curves (control mode FORCE, rate=2N/min). However, due to inconsistencies in sample thicknesses, these measurements did not yield consistent or conclusive results. Membranes were breaking at the edge of the UTM clamp (see Figure A.4b), instead of breaking in the middle which lead to faulty measurement.

One of the measurements from the commercial thick membranes is shown in Figure A.5. Samples prepared and experimented are shown in the Figure A.5.

To have more accurate results, similarly to DMA, it is recommended to have slightly thicker dry samples, above 70 μm.

Overall, we believe that conducting mechanical characterization experiments would reveal the suitability of membranes for commercial application, ideally showing the values for $TS > 15MPa$ and $EB > 100\%$. [23]

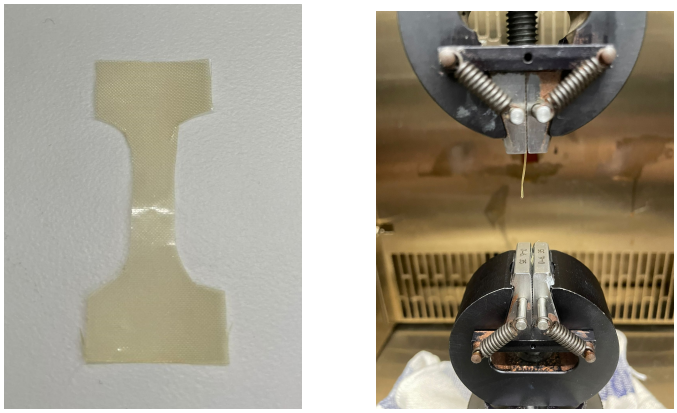

(a) UTM sample shape **(b)** UTM clamps

Figure A.4: (a) UTM sample shape and (b) UTM Clamps with Faulty Fracture of the Sample

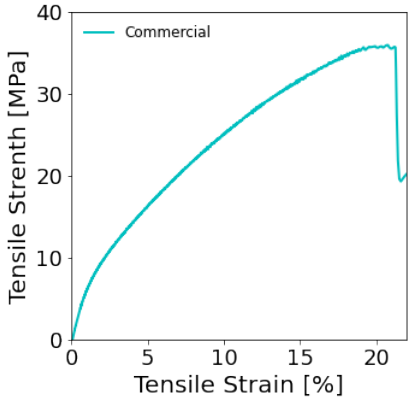

Figure A.5: Stress-strain curve of commercial membrane

A.2.4. DSC

DSC has already been used as a polymer characterization method, providing the glass transition temperature for the polymer solution. However, assuming formation of alignment during applying DC electric field, we could say that polymer membranes behave as semi-crystalline materials with distinguished amorphous and crystalline domains. If this is the case, DSC should be able to detect different glass transition temperatures for amorphous phases for different samples. It is believed that rise in crystalline phase induces rise in glass transition temperature. This can be explained by the decreased flexibility of amorphous domains when the density of the crystalline structure increases. [66]
DSC analysis was conducted on different samples, but clear phase transition peaks were not always observed. Figure A.6 shows the glass transition temperature for the polymer solution and the membrane cast at $1V$ DC voltage, indicating a significant increase in value. This would follow the expected trend; higher alignment in the polymer morphology would lead to higher value of glass transition temperature.

Additional experimental graphs are presented in Figure A.7. DSC graphs showed inconsistent and low-intensity peaks, probably due to the low mass of the samples and the presence of impurities. It is suggested to decrease the heating and cooling rates to achieve more observable peaks.

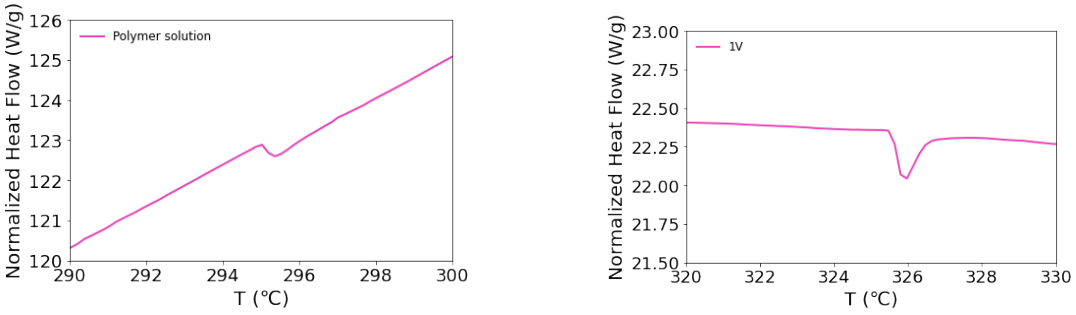

(a) T_g for polymer solution

(b) T_g for $1V$ DC

Figure A.6: DSC: Difference in glass transition temperature due to increased crystallinity

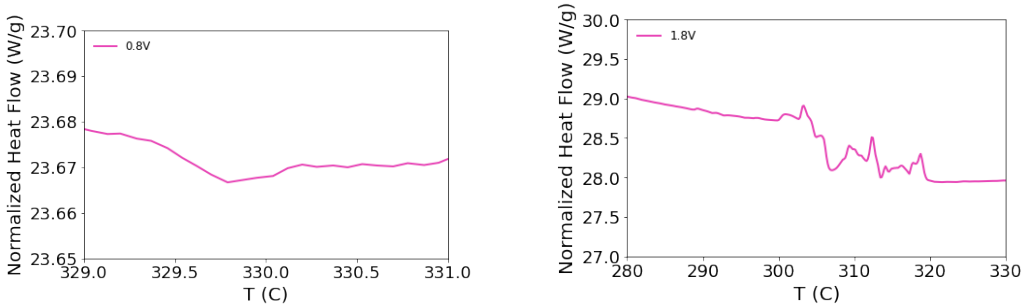

(a) Caption for the first figure

(b) Caption for the second figure

Figure A.7: DSC analysis for 0.8V and 1.8 V DC voltage membranes

A.2.5. XPS

XPS is a measurement which can indicate oxidation state of elements in the molecules by calculating binding energy of electrons. Binding energy represents energy required to remove an electron from specific atomic orbital to outside of the atom. [67] FTIR analysis indicated change of the oxidation state of nitrogen at higher applied DC voltages. Indeed, this could be observed on XPS spectra for $N1s$ orbital, at binding energies of 400eV for tertiary nitrogen and 402.4 eV for quaternary nitrogen. [67]

Spectra for different samples is given in the figure A.8b. It is important to indicate that measurement for pristine and 2V DC membrane was done with XPS equipment available at *Mechanical Engineering Department*, whereas other samples were analyzed at the *Faculty of Applied Sciences*. Count rate of detected photoelectrons (y-axis) has been normalized in the similar way as for WAXS data, from 0-1.

Previously, FTIR confirmed the protonation of available tertiary nitrogen atoms, which could result in a decrease in the XPS peak at 400 eV for membranes with higher IEC. Figure (b) A.8b for the 2V DC voltage membrane may indicate complete quaternization of nitrogen groups, aligning with this observation. Furthermore, the sample for 2V DC was taken from a section of the membrane that turned brown during casting. The observed complete quaternization might explain this phenomenon, but further analysis should prove this.

However, Figure (a) A.8b with other DC voltage samples showed an inconsistent trend. We believe this inconsistency is due to the preparation of samples from different polymer batches, probably with varying compositions of tertiary nitrogen.

Therefore, future research should focus on consistent sample preparation and confirmation of chemical structural change at higher DC voltages.

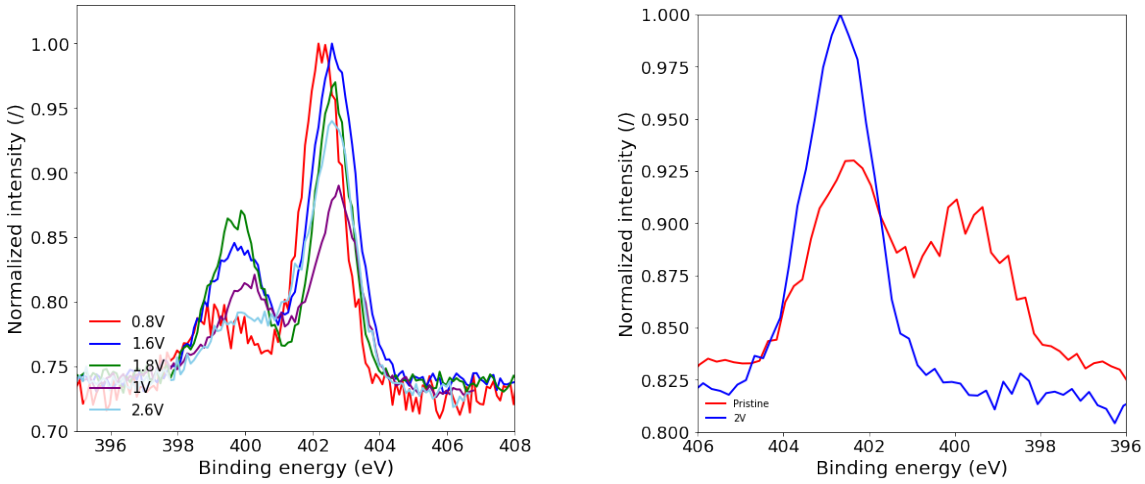

(a) XPS various DC voltage samples

(b) Extreme voltage ranges

Figure A.8: XPS analysis

A.2.6. SAXS

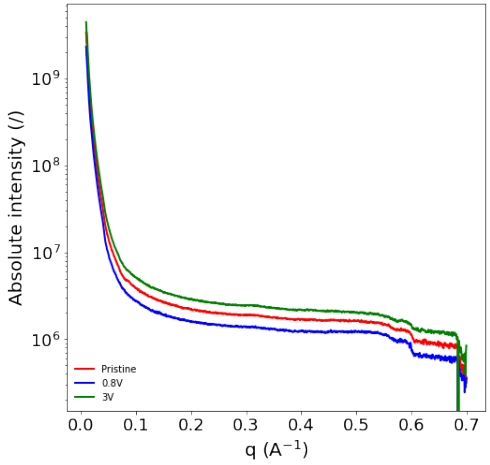

Figure A.9: SAXS absolute intensity

A.2.7. IEC

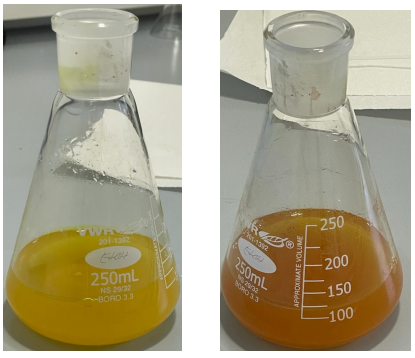

(a) Yellow solution

(b) Red/brown solution

Figure A.10: Colour change during IEC titration

A.2.8. Electrochemical characterization

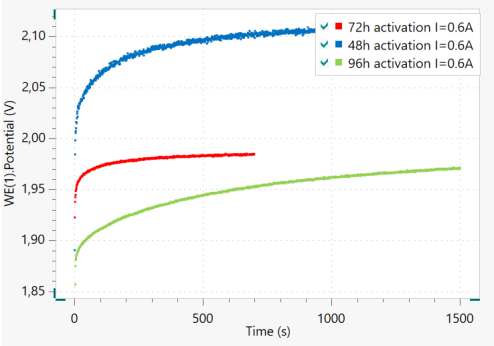

Figure A.11: Impact of Different Activation Times in 1M KOH on Commercial Sustainion Membrane

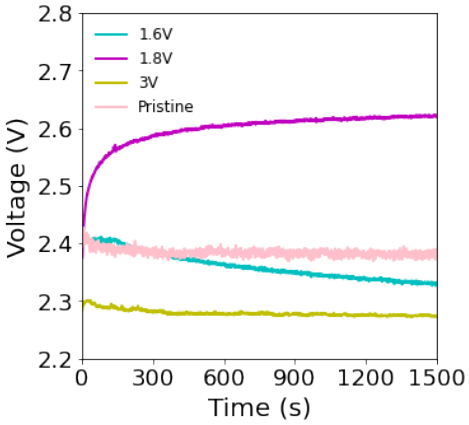

(a) CP room T $50 \pm 2\mu m$

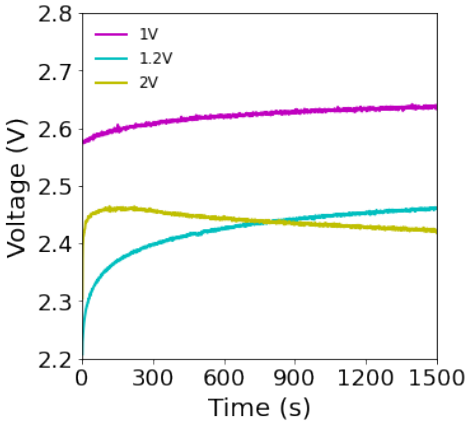

(b) CP room T $60 \pm 4\mu m$

Figure A.12: Comparison of Chronopotentiometry curves at room T